Cell

Distinct *in vivo* dynamics of donor-derived stem cell memory CAR T cells post-allogeneic HSCT relapse

Graphical abstract

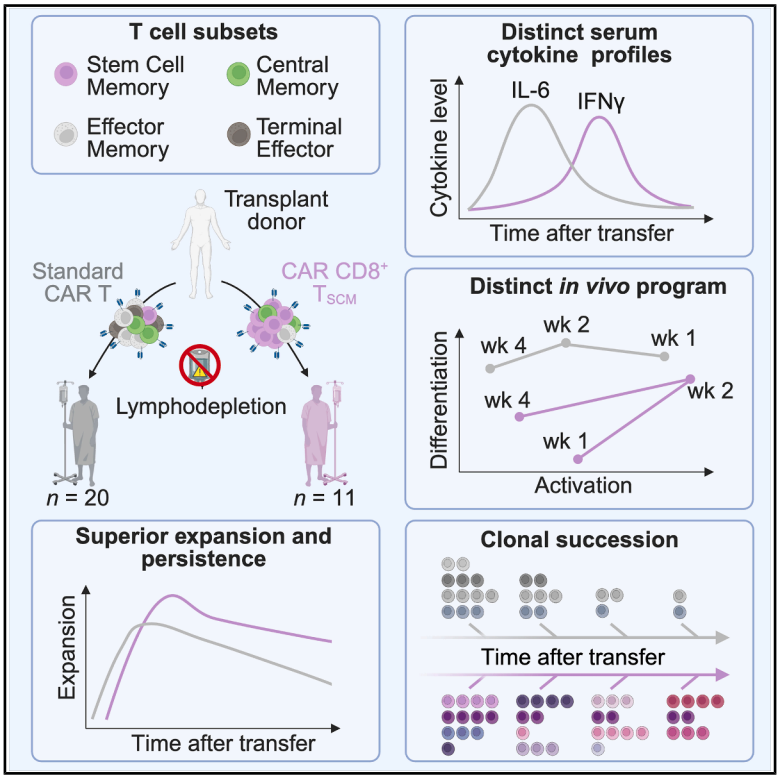

Authors

Luca Gattinoni, Gabriele Inchingolo, Dennis C. Harrer, ..., Enrico Lugli, Jennifer N. Brudno, James N. Kochenderfer

Correspondence

luca.gattinoni@lit.eu (L.G.), kochendj@mail.nih.gov (J.N.K.)

In brief

Donor-derived CD8⁺ CAR T_{SCM} cells exhibit enhanced expansion and a favorable safety profile, inducing complete responses at low doses without lymphodepletion. Their distinctive *in vivo* behavior and differentiation trajectory establish T_{SCM} cells as a robust and safe platform for next-generation CAR T cell therapy.

Highlights

- CAR T_{SCM} cells expand and persist longer, achieving complete responses at low doses
- CAR T_{SCM} cells induce mild cytokine release syndrome, primarily driven by IFN-γ
- CAR T_{SCM} cells exhibit distinct *in vivo* dynamics, repopulating the T_{SCM} compartment
- CAR T_{SCM} maintenance is sustained by clonal succession waves

Gattinoni et al., 2026, Cell *189*, 1–15
June 11, 2026
https://doi.org/10.1016/j.cell.2026.03.047

CellPress

Please cite this article in press as: Gattinoni et al., Distinct *in vivo* dynamics of donor-derived stem cell memory CAR T cells post-allogeneic HSCT relapse, Cell (2026), https://doi.org/10.1016/j.cell.2026.03.047

Cell

CellPress
OPEN ACCESS

Article

Distinct *in vivo* dynamics of donor-derived stem cell memory CAR T cells post-allogeneic HSCT relapse

Luca Gattinoni,[1,2,3,4,15,16,*] Gabriele Inchingolo,[1,15] Dennis C. Harrer,[5] Alberto Susana,[6] Simone Puccio,[6,7] Dragana Slavkovic-Lukic,[1] Danielle A. Natrakul,[8] Nicholas Strieder,[9] Christoph Heuser-Loy,[1] Jeremy G. Baldwin,[1] Jessica Fioravanti,[1,2] Yun Ji,[2] Sanjivan Gautam,[2] Chiara Suriano,[10] Azucena Martín-Santos,[1] Roland C. Schelker,[1,5] Nisha Patel,[11] Jennifer Mann,[8] Stephanie Goff,[8] Lekha Mikkilineni,[12] James C. Yang,[8] Mei Li M. Kwong,[8] Rashmika Patel,[2] Michael Rehli,[5,9] Steven L. Highfill,[13] David F. Stroncek,[13] Steven A. Rosenberg,[8] Luca Biasco,[14] Enrico Lugli,[6] Jennifer N. Brudno,[8,15] and James N. Kochenderfer[8,15,*]

[1]Division of Functional Immune Cell Modulation, Leibniz Institute for Immunotherapy, Regensburg, Germany
[2]Center for Cancer Research, National Cancer Institute, National Institutes of Health, Bethesda, MD, USA
[3]University of Regensburg, Regensburg, Germany
[4]Center for Immunomedicine in Transplantation and Oncology, University Hospital Regensburg, Regensburg, Germany
[5]Department of Internal Medicine III, Hematology and Oncology, University Hospital Regensburg, Regensburg, Germany
[6]IRCCS Humanitas Research Hospital, Rozzano, Italy
[7]Institute of Genetics and Biomedical Research, Milan Unit, Consiglio Nazionale delle Ricerche, Rozzano, Italy
[8]Surgery Branch, National Cancer Institute, National Institutes of Health, Bethesda, MD, USA
[9]Next Generation Sequencing Core, Leibniz Institute for Immunotherapy, Regensburg, Germany
[10]Epigenetic Immuno-Oncology Group, Leibniz Institute for Immunotherapy, Regensburg, Germany
[11]Hematology Section, Department of Laboratory Medicine, National Institutes of Health, Clinical Center, Bethesda, MD, USA
[12]Division of Bone and Marrow Transplantation & Cellular Therapies, Stanford University School of Medicine, Palo Alto, CA, USA
[13]Department of Transfusion Medicine, National Institutes of Health, Clinical Center, Bethesda, MD, USA
[14]Faculty of Population Health Science, Department of Infection Immunity and Inflammation, Zayed Centre for Research, University College of London, London, UK
[15]These authors contributed equally
[16]Lead contact
*Correspondence: luca.gattinoni@lit.eu (L.G.), kochendj@mail.nih.gov (J.N.K.)
https://doi.org/10.1016/j.cell.2026.03.047

SUMMARY

Donor-derived CD19-CAR T cells offer a therapeutic option for B cell malignancies relapsing after allogeneic hematopoietic stem cell transplantation but are often constrained by poor engraftment, expansion, and persistence. In a first-in-human study (NCT01087294), we found that CAR-modified stem-cell memory T (T_{SCM}) cells exhibited greater expansion and persistence than standard CAR T cells, enabling complete responses at low doses in the absence of lymphodepletion. CAR T_{SCM} cells induced mild cytokine-release syndrome, dominated by IFN-γ. Both products differentiated into effectors; however, only CAR T_{SCM} cells robustly reconstituted the stem-like compartment over time. CAR T_{SCM} cells were sustained through clonal succession, whereas persisting standard CAR T cells resulted from maintenance or contraction of early-expanded clones. While poor expansion limited standard CAR T cell activity, resistance to CAR T_{SCM} cells was driven primarily by tumor- and host-related factors. These findings establish CAR T_{SCM} cells as a promising platform for next-generation CAR T cell therapies.

INTRODUCTION

Over the past three decades, allogeneic hematopoietic stem cell transplantation (alloHSCT) has become a life-saving treatment for advanced B-cell malignancies. However, relapse remains the leading cause of mortality, accounting for approximately 60% of deaths occurring beyond 100 days post-transplant.[1] Donor lymphocyte infusion (DLI) has been employed as salvage therapy for post-alloHSCT relapse,[2] but low response rates and a high incidence of graft-versus-host disease (GvHD) have limited its use.[3] Re-directing donor-derived T cell specificity with chimeric antigen receptors (CARs) may overcome these limitations by enhancing the graft-versus-leukemia potency of allogeneic T cells without worsening GvHD.[4] Nonetheless, in the absence of lymphodepletion, donor-derived CAR T cells often show poor engraftment, limited

Please cite this article in press as: Gattinoni et al., Distinct *in vivo* dynamics of donor-derived stem cell memory CAR T cells post-allogeneic HSCT relapse, Cell (2026), https://doi.org/10.1016/j.cell.2026.03.047

expansion, and reduced persistence, resulting in modest objective responses.[5,6]

Retrospective studies have demonstrated a strong association between early memory T cell frequency and clinical responses after CAR T cell therapy.[7–9] Among these subsets, stem-cell memory T (T_{SCM}) cells, a minimally differentiated population endowed with self-renewal and multipotency, stand out for their robust proliferative capacity, long-term survival, and potent antitumor activity, making them an ideal cell type for adoptive immunotherapy.[10–12] Higher frequencies of T_{SCM} cells in CAR T cell products correlate with greater CAR T cell expansion[13] and improved clinical outcomes.[14] However, T_{SCM} cells comprise only a small fraction of current CAR T cell products and their therapeutic relevance has yet to be validated prospectively.

We previously developed a clinical-grade platform for generating CAR-modified T_{SCM} cells and demonstrated superior anti-leukemic activity against acute lymphoblastic leukemia (ALL) xenografts.[15] To translate these findings clinically, we amended a phase 1 trial of donor-derived CD19-CAR T cells in patients with relapsed or refractory $CD19^+$ malignancies post-alloHSCT (NCT01087294),[6] allowing the treatment of a second cohort with a T_{SCM}-enriched CAR T cell product. CAR T cells were administered without chemotherapy-based conditioning, enabling a direct assessment of the T cell products without confounding effects from other treatments. Here, we present clinical outcomes and in-depth immunomonitoring of the two cohorts, assessing whether the T_{SCM} cell platform improves safety and efficacy over conventional CAR T cell products, and providing mechanistic insights into distinct biology.

RESULTS

CAR T_{SCM} products exhibit high uniformity

Donor-derived CD19 CAR T_{SCM} cells were generated using a previously established manufacturing protocol[15] and compared with standard CAR T cell products.[6] A schematic overview of both manufacturing processes is shown in Figure 1A. Standard CAR T cells were generated by activating peripheral blood mononuclear cells (PBMCs) with soluble anti-CD3 and IL-2 following a protocol analogous to that used for axicabtagene ciloleucel.[6,16] As previously reported,[15] CAR T_{SCM} cells were manufactured from enriched *naive* $CD8^+$ T cells stimulated with CD3/CD28 microbeads. Culture conditions included IL-7 to promote T_{SCM} cell differentiation,[17] IL-21 to limit effector T cell maturation,[18,19] and the glycogen synthase kinase 3 beta (GSK-3β) inhibitor TWS119 to enhance WNT signaling[10,11,15,20] and stabilize stemness-associated transcriptional programs.[21,22] While the standard manufacturing process generated a more balanced ratio of $CD8^+$ and $CD4^+$ T cells (mean ± SD: 54.7% ± 17.3% versus 41.4% ± 17.1%, respectively) (Figures 1B and 1C), T_{SCM} culture conditions, by design, yielded an almost exclusively $CD8^+$ T cell population (mean ± SD: 98.7% ± 1.1%). CAR T_{SCM} products were highly enriched in T_{SCM} cells compared with those generated with the standard procedure (median: 78.4% versus 8.4%), whereas standard CAR T cells were more heterogeneous, with predominant proportions of effector memory (T_{EM}) and terminal effector (T_{TE}) cells (median: 34.2% and 21%, respectively) (Figure 1D). Phenograph clustering[23] identified 10 distinct clusters within the two CAR T cell products (Figures 1E–1G). Notably, CAR T_{SCM} cells were almost entirely confined to clusters 4, 6, 8, and 9, which exhibited the hallmark T_{SCM} phenotypic traits, with only minor expression-level variations. In contrast, clusters 2, 3, and 5, which comprise cells with a T_{EM}-like profile, were primarily restricted to standard CAR T cells (Figures 1E–1G). These findings indicate that T_{SCM} culture conditions result in highly homogeneous CAR T_{SCM} products, whereas the standard process yields a heterogeneous product enriched in effector subsets.

Superior CAR T_{SCM} expansion yields complete responses at low doses

The total CAR T cell doses administered in the two cohorts are illustrated in Figure 2A and summarized in Tables S1 and S2. The standard cohort received significantly higher CAR T cell numbers compared with T_{SCM} recipients (median: 290 million versus 66 million, respectively) (Figure 2A). Despite lower doses, CAR T_{SCM} recipients achieved overall response rates (ORRs) comparable with those of standard patients (55% versus 45%, respectively) (Figure 2B). There was no significant difference in event-free survival (EFS), with a median EFS of 3.3 months in the standard CAR T cell cohort and 4.9 months in the CAR T_{SCM} cohort (Figure 2C). Among the four T_{SCM} recipients with EFS > 24 months (patient number [Pt #] 22, 25, 27, and 28), CD19 expression was assessed before treatment and at relapse in three patients; in two of these cases, CD19 expression was uniformly present before treatment but was dim (Pt #22) or absent on the majority of relapsing leukemic cells (Pt #27), suggesting antigen escape under CAR T cell immune pressure. Notably, at a comparable dose range ($<3 \times 10^8$ CAR T cells), CAR T_{SCM} cells demonstrated improved activity, with complete responses observed in 5 out of 11 patients (45%), versus 1 out of 10 patients (10%) in the standard cohort ($p = 0.0362$, one-tailed chi-squared test) (Figures 2A and 2B). Examples of outcomes induced by CAR T_{SCM} cells are shown in Figures 2D–2F, highlighting complete radiological (Figure 2D) and pathological (Figure 2E) responses in two ALL patients. Importantly, CAR T_{SCM} cells were able to elicit anti-tumor responses in peripheral tissues, as demonstrated by the dramatic regression of an extramedullary ALL cutaneous mass (Figure 2F).

CAR T cell peak expansion and overall exposure—measured as area under the curve (AUC)—have been associated with responses.[24–27] Therefore, we evaluated the absolute number of circulating CAR T cells by qPCR during the first 36 days post-infusion. We found that CAR T_{SCM} cells exhibited a delayed expansion, peaking in the second week post-infusion, compared with standard CAR T cells, which peaked within the first week (Figures 2G and S1). This pattern aligns with recent observations that later waves of CAR T expansion arise from cells within the infusion product that possess a stem-like signature.[28] T_{SCM} recipients exhibited a higher per-cell peak blood level of CAR T cells (median: 30.4 CAR T cells/μL) compared with standard patients (median: 6.7 CAR T cells/μL) (Figure 2G) as well as a higher per-cell $AUC_{d0\text{-}36}$ (median: 185.8 CAR T cells/μL versus 27.5 CAR T cells/μL) (Figures 2G and 2H). qPCR results

Please cite this article in press as: Gattinoni et al., Distinct *in vivo* dynamics of donor-derived stem cell memory CAR T cells post-allogeneic HSCT relapse, Cell (2026), https://doi.org/10.1016/j.cell.2026.03.047

CellPress
OPEN ACCESS

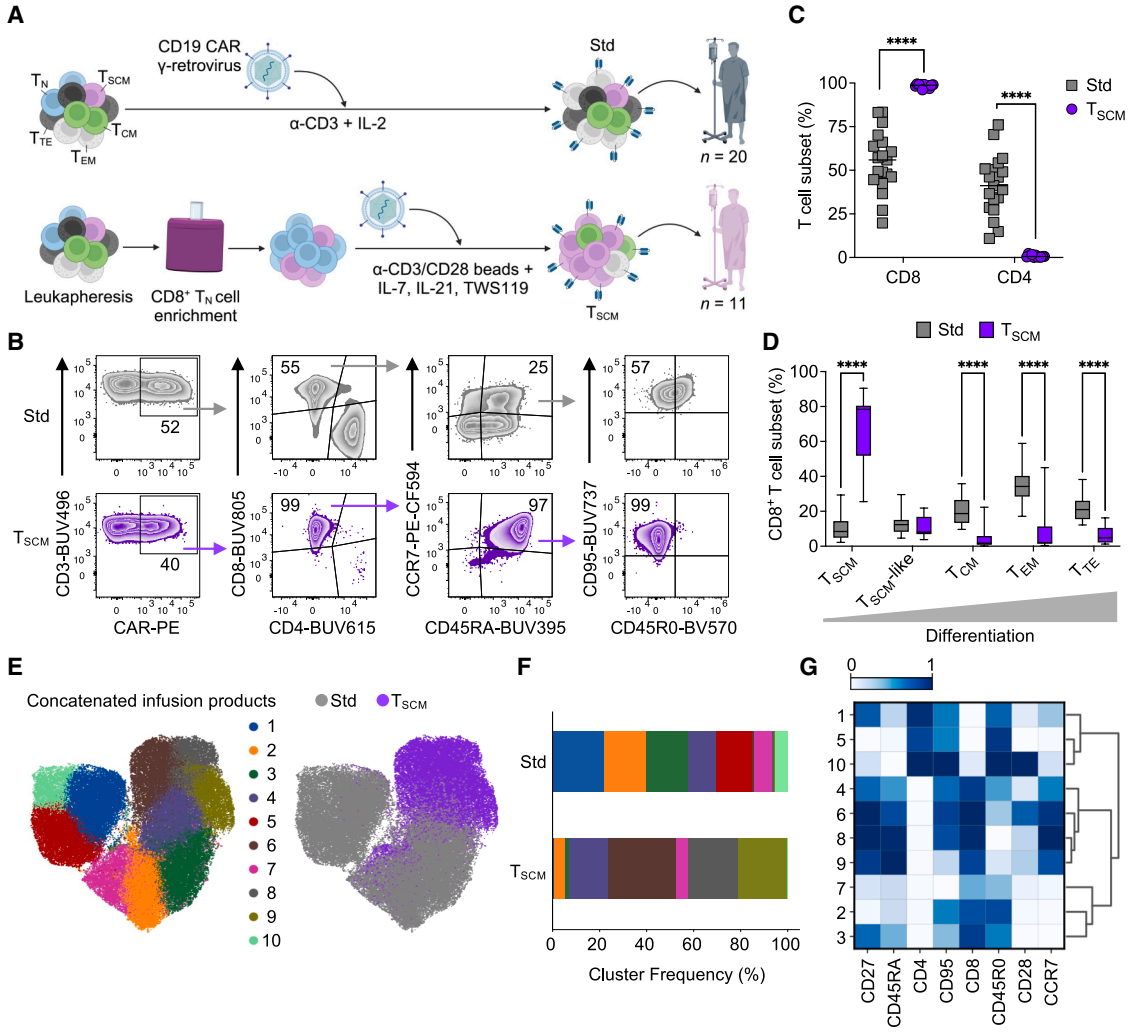

Figure 1. CAR T_{SCM} products exhibit greater phenotypic uniformity than standard CAR T cells

(A) Schematic representation of the manufacturing processes for standard (top) and CAR T_{SCM} manufacturing (bottom). T_N, *naive*; T_{SCM}, stem cell memory; T_{CM}, central memory; T_{EM} effector memory; and T_{TE}, terminal effector.

(B) Flow cytometry gating strategy used to characterize the standard and T_{SCM} CAR product compositions. T_{SCM} were defined as $CCR7^+CD45RA^+CD45R0^-CD95^+$; T_{CM} as $CCR7^+CD45RA^-$; T_{EM} as $CCR7^-CD45RA^-$; T_{TE} as $CCR7^-CD45RA^+$; T_{SCM}-like cells as $CCR7^+CD45RA^+$. Numbers indicate the percentage of cells in each quadrant.

(C and D) (C) Percentage of $CD8^+$, $CD4^+$ T cells, and (D) distribution of indicated subsets within both products. Data are shown after gating on live $CD3^+CAR^+$ cells. Results from standard (n = 19) and T_{SCM}-enriched (n = 11) CAR T cell products are shown as box-and-whisker plots. Boxes indicate the median and interquartile range with whiskers extending up to 1.5 times the interquartile range (****$p < 0.0001$; multiple t test, Holm-Šídák correction for multiple comparisons).

(E) UMAP plots of concatenated CAR T cell products showing cluster identity (left) and treatment group distribution (right). Data on UMAP are shown after gating on live $CD3^+CAR^+$ cells.

(F) Stacked bar graph showing the percentage of each cluster in standard and T_{SCM}-enriched CAR T cell products.

(G) Heatmap of the relative expression (z score) of memory markers in each cluster. Hierarchical clustering (dendrogram) highlights similarities and differences between clusters.

were validated by flow cytometry, confirming the delayed (Figures S1A and S1B) and higher expansion of CAR T_{SCM} cells (median: 7.3% versus 1%) (Figures 2I and 2J). To assess whether these differences in CAR T cell expansion could be attributed to variability in lymphodepletion due to the interval from prior therapies (Tables S3 and S4), we evaluated baseline $CD3^+$ T cell and NK cell counts. With the exception of one patient in the standard CAR T cell group showing marked T cell depletion, all other patients had $CD3^+$ and NK cell levels within or close to normal limits (Figures S1C and S1D). Importantly, there were no significant differences in baseline lymphocyte counts between the two cohorts. Thus, the delayed kinetics and greater expansion observed in the CAR T_{SCM} cohort likely reflect intrinsic biological properties of the infused cells rather than differences

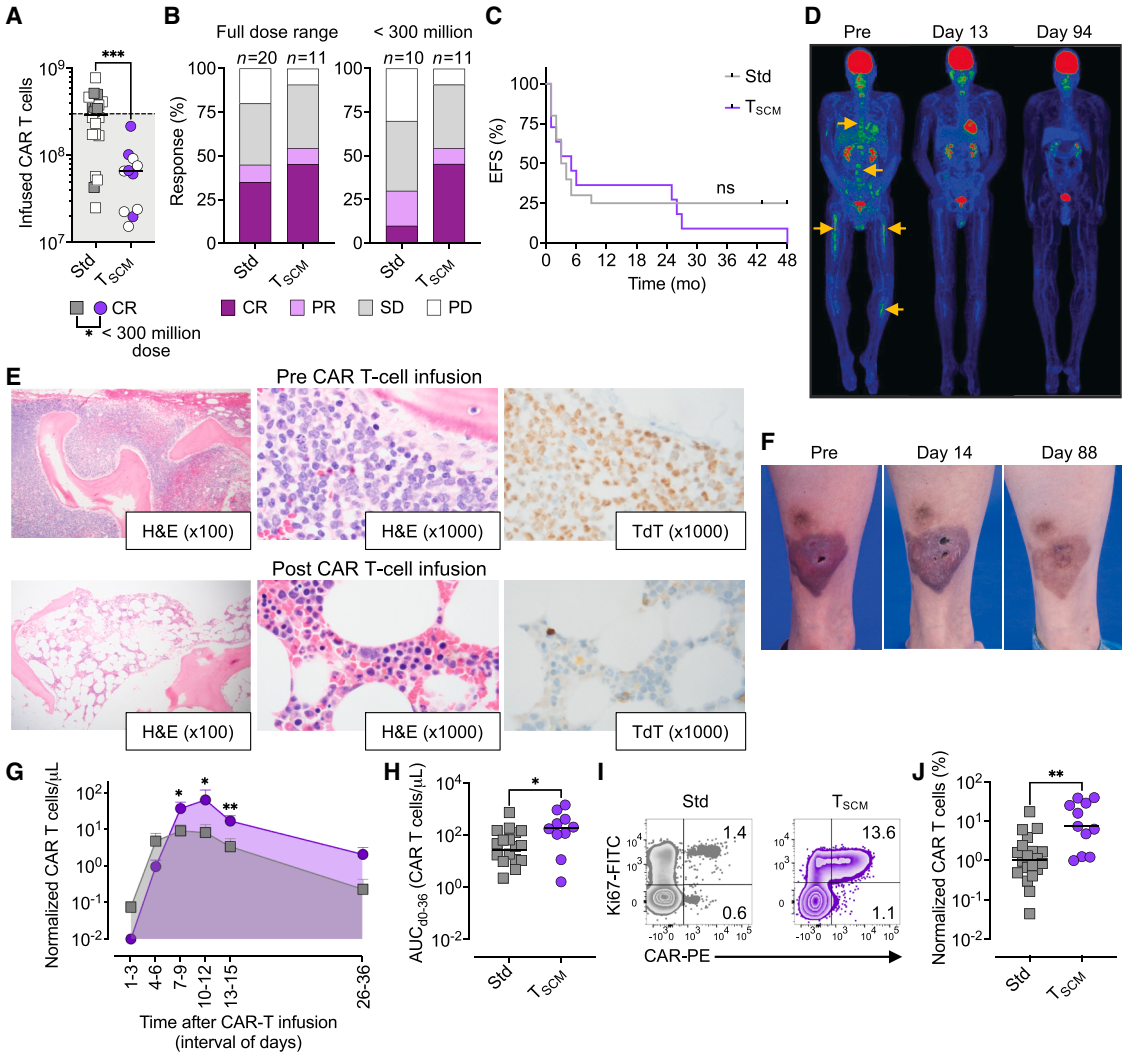

Figure 2. Enhanced expansion and persistence of CAR T_{SCM} cells drive superior responses at lower doses

(A) Total dose range of infused CAR T cells in standard ($0.4–8.2 \times 10^6$ kg^{-1}, $n = 20$) and T_{SCM} ($0.25–2 \times 10^6$ kg^{-1}, $n = 11$) cohorts for first cell infusions. Doses below the black-dashed line in the gray box correspond to dose values $<3 \times 10^8$ infused CAR T cells. Empty and filled symbols represent non-complete and complete responders, respectively. Data are shown as individual values, while horizontal black bars represent median values (*$p < 0.05$, one-tailed chi-squared test [proportion of CRs for $<3 \times 10^8$ infused CAR T cells]; *** $p < 0.001$, two-tailed Mann-Whitney test [comparison of CAR T infusion doses]).

(B) Best response rates (%) to first infusion in standard and T_{SCM} recipients, shown for the full dose range (left) and doses $<3 \times 10^8$ (right) infused CAR T cells. CR, complete response; PR, partial response; SD, stable disease; and PD, progressive disease.

(C) Event-free survival (EFS) post-CAR T cell infusion in standard versus T_{SCM} recipients for first infusions. ns = not significant (log-rank test).

(D) PET/CT images showing progressive resolution of multiple fluorodeoxyglucose (FDG)-avid B-cell ALL bone lesions (yellow arrows) in Pt #28 following the infusion of CAR T_{SCM} cells.

(E) Bone marrow hematoxylin and eosin (H&E) staining (left and middle) and terminal deoxynucleotidyl transferase (TdT) staining (right) for Pt #31 demonstrating 90% B-cell ALL involvement pre-treatment (top row) and hypocellular marrow with trilineage hematopoiesis and no morphologic evidence of B-ALL (bottom row) 36 days after infusion of CAR T_{SCM} cells. Immunohistochemical images are shown at 100× (left panels) and 1,000× magnification (center and right panels).

(F) Pre- (left) and post-treatment photographs (middle, right) of a biopsy-proven extramedullary B-cell ALL cutaneous lesion in Pt #29 showing gradual evolution and improvement following the first infusion of CAR T_{SCM} cells.

(G) Absolute circulating CAR$^+$ T cell numbers per microliter of blood assessed by qPCR. Cells are normalized to the total infused dose (per 10^8 infused cells). Data are grouped into 3-day intervals (*$p < 0.05$; **$p < 0.01$, two-tailed Mann-Whitney test).

(H) Area under the curve (AUC) from day 0 to day 36 post-infusion (*$p < 0.01$, two-tailed Mann-Whitney test).

(I) Flow cytometry plot showing the frequency of proliferating CAR T cells at the peak of expansion as assessed by Ki67 staining in Pt #14 (standard) and #27 (T_{SCM}). Numbers indicate the percentage of cells in each quadrant.

(J) Frequency of CAR T cells in peripheral blood at the peak of expansion in standard and T_{SCM} recipients. Cells are normalized to the total infused dose (per 10^8 infused cells); (** $p < 0.01$, two-tailed Mann-Whitney test).

See also Figure S1.

Please cite this article in press as: Gattinoni et al., Distinct *in vivo* dynamics of donor-derived stem cell memory CAR T cells post-allogeneic HSCT relapse, Cell (2026), https://doi.org/10.1016/j.cell.2026.03.047

in lymphodepletion.[29,30] Together, these findings suggest that the superior complete responses achieved by CAR T_{SCM} cells at low doses are driven by their enhanced capacity for expansion and persistence.

CAR T_{SCM} cells exhibit a favorable safety profile

The administration of donor-derived CAR T_{SCM} cells was well tolerated, with no GvHD and a low incidence of cytokine release syndrome (CRS) or other severe adverse events (Tables S1 and S5). No grade 4 (G4) CRS events were observed in the T_{SCM} cohort. Only one patient with 40%–50% ALL blast infiltration in the bone marrow (BM) developed grade 3 (G3) CRS. In contrast, 28.6% of patients treated with standard CAR T cells experienced grade 3–4 CRS toxicities (Figure 3A, left). Of note, these differences were maintained when comparing patients who received comparable dose levels (Figure 3A, right). Consistent with prior reports,[25,31] CRS severity correlates with CAR T cell expansion in our standard cohort, in which G3-4 toxicities occurred in patients who exhibited higher peak expansion compared with those with G1-2 CRS (Figure 3B), with no clear correlation with $CD4^+$ versus $CD8^+$ T cell expansion (Figure S2A). Remarkably, CAR T_{SCM} cell recipients, who experienced peak expansion levels comparable with those observed in patients with G3-4 CRS in the standard cohort, displayed only G1-2 toxicities, suggesting that CAR T_{SCM} products uncouple expansion from toxicity (Figure 3B). Responder patients in both cohorts developed fever following CAR T cell infusion. In the standard cohort, fever occurred during the first week post-infusion, whereas in the T_{SCM} cohort it emerged in the second week (Figure 3C), consistent with the delayed kinetics of CAR T cell expansion (Figure 2G). Despite both cohorts experiencing fever at similar temperatures, standard CAR T cell recipients showed heightened inflammatory responses, as evidenced by elevated levels of C-reactive protein (Figure 3D).

To determine whether the observed differences in CRS and inflammation between standard and T_{SCM} patients were associated with distinct cytokine patterns, we performed serum cytokine profiling. We observed elevated levels of interleukin-6 (IL-6) in the standard cohort immediately after CAR T cell infusion, which normalized by the end of the first week (Figure 3E). In contrast, the CAR T_{SCM} cell administration was primarily associated with a peak in interferon-γ (IFN-γ) during the second week, reflecting the distinct temporal dynamics of their *in vivo* expansion (Figure 3E). No differential patterns were observed for the other cytokines analyzed (Figure S2B). Interestingly, IL-6 levels correlated with CRS severity exclusively in the standard cohort, whereas IFN-γ emerged as the primary driver of toxicity in the T_{SCM} group (Figures 3F and 3G). The virtual absence of $CD4^+$ T cells—which play a major role in driving CRS[32–34] via licensing of monocytes/macrophages[35,36]—in the T_{SCM} cohort, along with differences in $CD8^+$ T cell subset composition[37] in the infusion product, may underlie the observed differences in serum cytokines and the favorable safety profile of CAR T_{SCM} therapy. To better understand the potential contribution of the $CD8^+$ T cell compartment in triggering CRS, we isolated $CD8^+CAR^+$ T cells from both infusion products and performed single-cell secretome analysis following stimulation with $CD19^+$ targets. Unsupervised cluster analysis identified 14 distinct clusters (Figure 3H). Consistent with our serum results, we observed a trend toward the enrichment of IL-6-secreting clusters (1 and 2) in the standard product, whereas clusters 11 and, to a certain extent, 14—marked by elevated IFN-γ secretion—were predominant in the CAR T_{SCM} cells (Figure 3I). Single-cell secretome analysis also revealed an increased presence of a highly polyfunctional cluster (3) within the CAR T_{SCM} products (Figure 3I). As polyfunctionality has previously been identified as a key determinant of antitumor responses,[38] this enrichment may have contributed to the enhanced therapeutic efficacy observed in the T_{SCM} cohort. Together, these findings suggest that the attenuated inflammatory response observed with CAR T_{SCM} therapy is shaped by its unique cytokine dynamics and profile.

CAR T_{SCM} cells exhibit distinct *in vivo* fates

To characterize the *in vivo* differentiation trajectories of standard and T_{SCM}-enriched CAR T cells, we performed high-dimensional flow cytometry on post-infusion samples using a 23-color panel encompassing canonical activation, differentiation, and exhaustion markers. Unsupervised clustering analysis identified 17 distinct clusters within the two cohorts (Figure 4A). T cell differentiation trajectories were then inferred using Slingshot.[39] Cluster 15, characterized by *bona fide naive* T (T_N) cells, was designated as the root cluster for trajectory reconstruction. We identified a primary differentiation path (white line) that progressed sequentially from T_N cells (clusters 15 and 4) to T_{SCM} cells (cluster 8), then to T_{CM} cells (cluster 9), followed by a transition to proliferating effectors (prol. T_{EFF}) (clusters 13, 6, 5, 11, and 10), and ultimately to resting T_{EFF} and T_{TE} cells (clusters 17, 2, 12, and 1) (Figure 4B). Wishbone analysis[40] was applied to define the expression dynamics of early, activation, and late differentiation markers along the inferred trajectory. The resulting expression trends were consistent with a progressive model of T cell differentiation reconstructed through pseudotime analysis (Figure 4C). Additionally, we performed principal component analysis (PCA) to further delineate specific T cell trajectories within the two cohorts at different time points following CAR T cell therapy (Figure 4D). T cell positioning at early time points (days 5–8) differed markedly between the T_{SCM} and standard cohorts. However, during the second week (days 9–11 and 12–14), the T_{SCM} trajectory gradually shifted toward the phenotypic state observed in the standard cohort on days 5–8 (Figure 4D). This observation aligns with the distinct expansion kinetics of the two products, with peak expansion occurring during the first week for standard CAR T cells and the second week for CAR T_{SCM} cells. Notably, the two trajectories further diverged along the PCA2 axis as cells transitioned to the memory phase (days 28–35) (Figure 4D). To dissect the phenotypic drivers of the PCA trajectory differences, we analyzed cluster contributions using vector projections in a biplot of the attributes (Figure S3A). Strong contributors included clusters 8 (T_{SCM}), 6, 14, 5, 11, and 10 (progressive stages of proliferating T_{EFF}), 3 (T_{EM}), 2 (resting T_{EFF}), and clusters 1 and 7 ($GZMB^+$ and $GZMK^+$ T_{TE}, respectively). CAR T_{SCM} cells exhibited delayed accrual into proliferating intermediate T_{EFF} cells, peaking at days 12–14, compared with standard CAR T cells, which reached this stage as early as days 5–8. By days 28–35, while standard CAR T cells were enriched in proliferating and resting late effector subsets, CAR T_{SCM} cells robustly repopulated the T_{SCM} compartment and the pool of very early proliferating T_{EFF} cells (Figures 4A, 4F, and

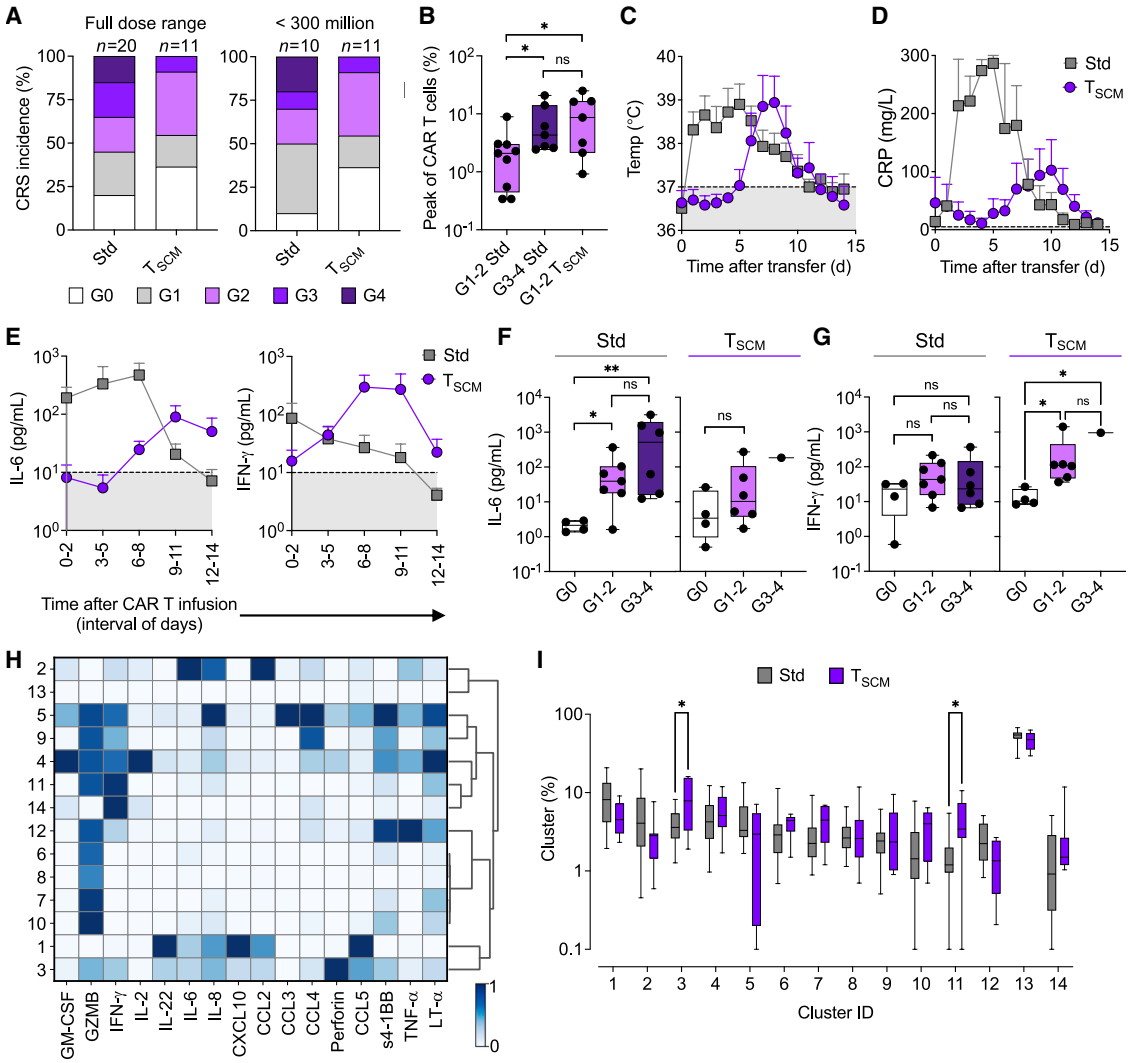

Figure 3. Reduced cytokine release syndrome severity following CAR T_{SCM} infusion

(A) CRS incidence in standard versus T_{SCM} recipients. Stacked bar graphs show CRS grades (G0–G4) after first cell infusions displayed for the full dose range (left) and doses $<3 \times 10^8$ infused CAR T cells (right).

(B) Correlation between the percentage of CAR T cells at the peak of expansion (measured by flow cytometry) and CRS severity (*$p < 0.05$, one-way ANOVA, Kruskal-Wallis test).

(C and D) Body temperature (C) and C-reactive protein (CRP) levels (D) in responder patients during the first two weeks after infusion of standard or T_{SCM}-enriched CAR T cells for the first cell infusions. Standard $n = 9$ (C) and 5 (D). T_{SCM} $n = 6$ (C and D).

(E) Serum levels of IL-6 (left) and IFN-γ (right) in responder patients over two weeks after infusion of standard or T_{SCM}-enriched CAR T cells. Time post-infusion is represented in day intervals. The gray box, outlined by a black dashed line, indicates the physiological reference levels of each cytokine. Standard $n = 7$. T_{SCM} $n = 6$.

(F and G) Serum peak levels of IL-6 (F) and IFN-γ (G) in standard ($n = 17$) and T_{SCM}-enriched ($n = 11$) CAR T cell recipients stratified according to CRS grade (*$p < 0.05$; **$p < 0.01$, one-way ANOVA, Kruskal-Wallis test).

(H) Heatmap showing the relative expression (Z score) of single-cell secreted cytokines by sorted CAR^+CD8^+ T cells from standard ($n = 20$) and T_{SCM}-enriched ($n = 8$) CAR T cell products after stimulation with $CD19^+$ K562. Clusters were identified using the VIA algorithm. Cluster 1 (983 cells) and cluster 14 (249) are the largest and least functional clusters, respectively.

(I) Relative contribution of each cluster within standard and T_{SCM} $CD8^+$ products. Cluster percentage was normalized to the total number of clusters per patient (*$p < 0.05$; **$p < 0.01$, multiple t test, Holm-Šídák correction for multiple comparisons).

See also Figure S2.

S3B). These findings highlight a distinct differentiation program in CAR T_{SCM} cells, characterized by delayed effector differentiation and sustained regeneration of stem-like cells and early memory precursors.

Clonal succession sustains long-term CAR T_{SCM} engraftment

To investigate the *in vivo* clonal dynamics of CAR T cells, we performed longitudinal tracking of retroviral integration sites (ISs)

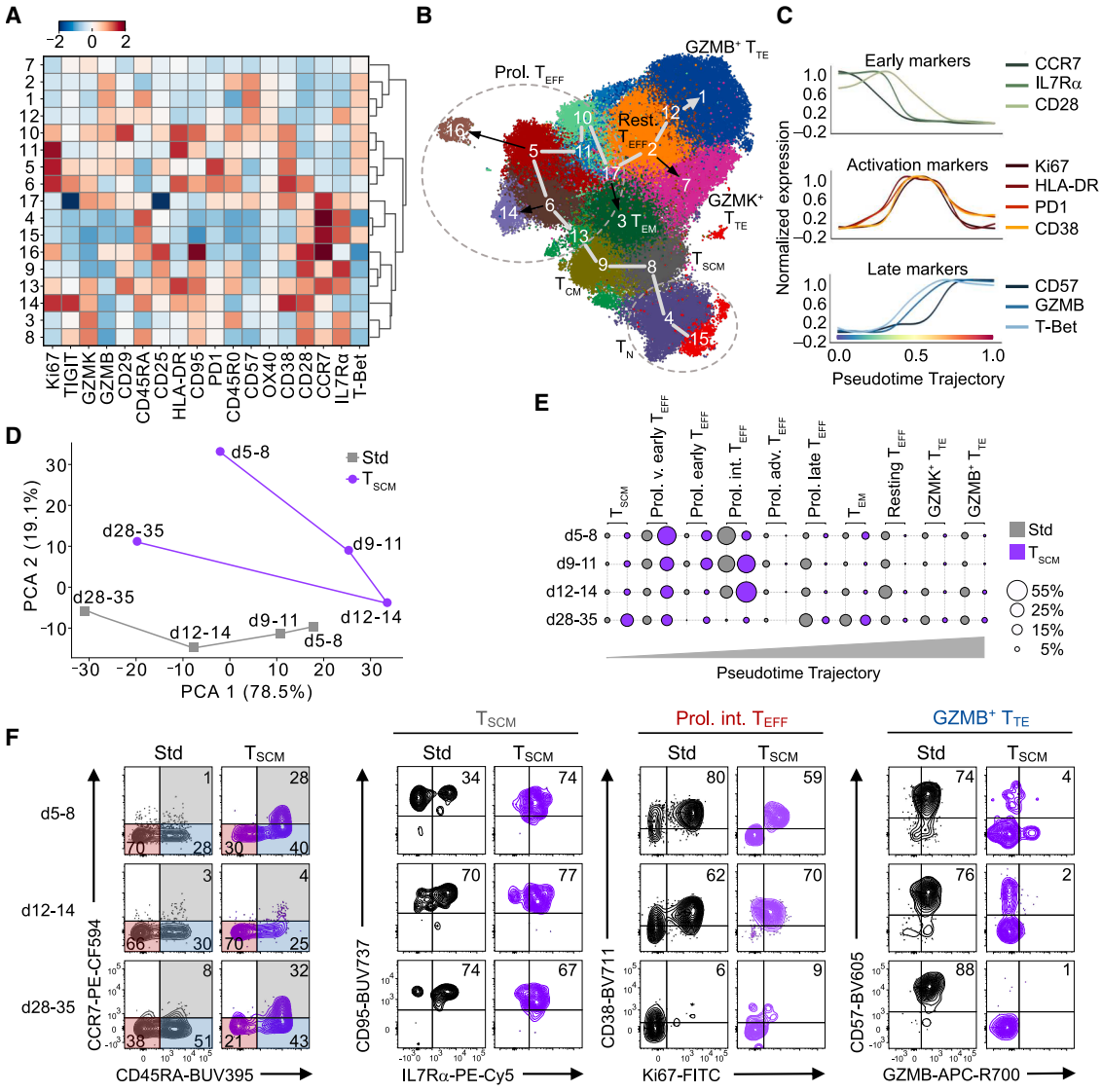

Figure 4. CAR T_{SCM} cells retain the ability to reconstitute the T_{SCM} compartment

(A) Heatmap showing the relative expression (*Z* score) of differentiation and activation markers in post-CAR T cell infusion samples from standard (n = 20) and T_{SCM}-enriched (n = 11) CAR T cell recipients. Clusters were identified using the VIA algorithm.

(B) Pseudotime reconstruction of $CD8^+$ T cell differentiation along the UMAP generated using post-infusion samples from standard and T_{SCM} recipients. A main inferred trajectory (white line) diverges into four minor differentiation branches (black arrows). Trajectories and branches were generated using the Slingshot package, assuming the T_N cluster (C_{15}) as the root.

(C) Normalized expression of early memory, activation, and late differentiation markers along the main pseudo time trajectory.

(D) Principal component analysis (PCA) of $CD8^+$ T cells in standard and T_{SCM} recipients at different time points following CAR T cell infusion.

(E) Bubble plot showing the frequencies of selected clusters obtained in (A) along the pseudo time trajectory shown in (B) at the indicated time points post-CAR T cell infusion. Bubble size indicates the frequency of each cluster over the pseudo time trajectory. T_{SCM} (C_8), Prol. v. early T_{EFF} (C_6), Prol. early T_{EFF} (C_{14}), Prol. int. T_{EFF} (C_5), Prol. adv. T_{EFF} (C_{11}), Prol. late T_{EFF} (C_{10}), T_{EM} (C_3), resting T_{EFF} (C_2), $GZMK^+$ T_{TE} (C_7), $GZMB^+$ T_{TE} (C_1).

(F) Flow cytometry plots showing T_{SCM}, proliferating intermediate T_{EFF}, and $GZMB^+$ T_{TE} subsets in two representative standard and T_{SCM} recipients (patients #18 and #29, respectively) at different time points following CAR T cell infusion. $CD95^+IL7R\alpha^+$ cells identify T_{SCM} cells (gray), $CD38^+Ki67^+$ cells mark Prol. int. T_{EFF} (red), and $CD57^+GZMB^+$ define T_{TE} (blue). Data are shown after gating on live $CD3^+CAR^+$ cells and $CCR7^+CD45RA^+$ (T_{SCM}), $CCR7^-CD45RA^-$ (Prol. int. T_{EFF}), and $CCR7^-CD45RA^+$ (T_{TE}) subsets. Numbers indicate the percentage of cells in each quadrant. T_{EFF}, effector T cells.

See also Figure S3.

within flow cytometry-sorted memory subsets from the infusion product to day 90 post-infusion (Figure S4A). To minimize potential confounding factors such as disease type and clinical outcome, we selected four ALL patients who achieved a minimal residual disease-negative (MRD^-) CR following treatment with either standard or T_{SCM}-enriched CAR T cells. We first evaluated the extent of

Please cite this article in press as: Gattinoni et al., Distinct *in vivo* dynamics of donor-derived stem cell memory CAR T cells post-allogeneic HSCT relapse, Cell (2026), https://doi.org/10.1016/j.cell.2026.03.047

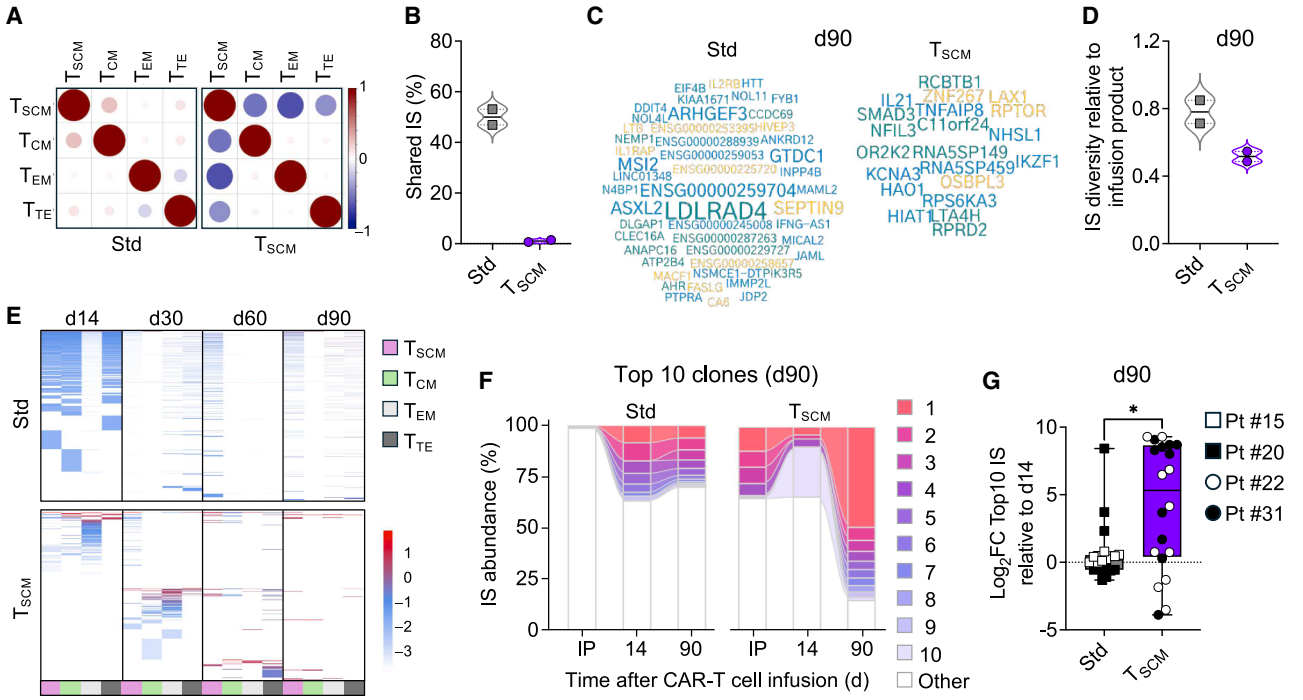

Figure 5. Long-term persistence of CAR T_{SCM} cells is sustained by clonal succession

(A) Correlation plots showing the degree of sharing of identical integration sites (IS) across each T cell subset in the standard (left) and T_{SCM} (right) CAR products from Pt #15 and #22, respectively. Positive and negative correlations are shown in red and in blue, respectively. The size of circles is proportional to the correlation value (Pearson correlation coefficient calculated between all pairs of variables).

(B) Violin plot showing the percentage of shared ISs found among the diverse T cell subsets within standard ($n = 2$) and T_{SCM} ($n = 2$) CAR products.

(C) Word clouds displaying the top 50 ISs loci at day 90 following CAR T cell infusion in Pt #15 (standard, left) and #22 (T_{SCM}, right). Each locus is labeled with the name of the closest gene to the relative insertion site. The size of each gene name is proportional to the number of integrations found at that locus, with larger fonts indicating higher integration frequencies.

(D) Shannon diversity index calculated on total ISs collected at day 90 post-CAR T cell infusion. A higher index indicates greater clonal diversity. Data are shown relative to the diversity index of the infusion products.

(E) Heatmap showing the longitudinal tracking of individual ISs within each T cell subset for Pt #15 (standard, top) and #22 (T_{SCM}, bottom). Each row represents an individual IS, and each column represents the T cell subset analyzed. The intensity of blue and red is proportional to the relative IS abundance, expressed as $\log_{10}$ percent sequencing read counts belonging to each IS for each sample/timepoint.

(F) Alluvial plots showing the abundance of top 10 clones persisting at day 90 in Pt #15 (standard, left) and #22 (T_{SCM}, right) backtracked to day 14 and the infusion product (IP). Ribbons connect identical ISs tracked over different time points (bars). The size of each ribbon/bar section is proportional to the relative IS abundance. The abundance of the rest of the ISs (other) is reported in the white section of each bar.

(G) Scatter plot showing the $\log_2$ fold change (FC) of the abundance top 10 ISs retrieved at day 90 relative to day 14 following CAR T cell infusion in standard ($n = 2$) and T_{SCM} ($n = 2$) recipients. The top 10 clones per patient are shown as individual values in box-and-whisker plots. Boxes indicate the median and interquartile range, with whiskers extending to 1.5 times the interquartile range (*$p < 0.05$, two-tailed Mann-Whitney test).

See also Figure S4.

shared ISs among memory subsets within the infused CAR T cell products. Interestingly, the T_{SCM} product showed minimal IS overlap across memory T cell populations, whereas the standard product exhibited a high degree of IS sharing (Figures 5A and 5B). The low number of shared ISs in the T_{SCM} product likely reflects the manufacturing conditions, which limit extensive proliferation while preserving stemness. Conversely, the high proportion of shared ISs in the standard CAR T cell product suggests that differentiation occurred during *in vitro* expansion. Importantly, the limited number of shared ISs in CAR T_{SCM} products enables more precise and less ambiguous tracking of specific IS clones over time from the original T_{SCM} compartment.

The overall clonal diversity of CAR T cells was reduced in T_{SCM} recipients after infusion at late time points compared with standard CAR T cell recipients. This outcome was expected since, as discussed above, the T_{SCM} patients received fewer cells than with the standard protocol. However, no evidence of clonal dominance or aberrant selection was observed, supporting the safety of T_{SCM} cells. (Figures 5C, 5D, and 4B.) To delineate the reconstitution dynamics of standard and T_{SCM} products, we longitudinally tracked individual clones while simultaneously analyzing their contribution to distinct T cell subsets. Standard CAR T cell clonotypes underwent rapid expansion post-infusion, followed by a contraction and/or stabilization over time (Figure 5E). Accordingly, the top 10 most abundant persisting clones at 90 days were derived from attrition or maintenance of early expanded (d14) clones (Figures 5F and 5G). In sharp contrast, CAR T_{SCM} cell repopulated the patient through

Please cite this article in press as: Gattinoni et al., Distinct *in vivo* dynamics of donor-derived stem cell memory CAR T cells post-allogeneic HSCT relapse, Cell (2026), https://doi.org/10.1016/j.cell.2026.03.047

sequential waves of clonal succession (Figure 5E). Notably, the top 10 most abundant persisting clones in T_{SCM}-treated patients emerged from newly expanded clones that were not involved in the initial expansion phase (Figures 5F and 5G). This pattern is reminiscent of the reconstitution dynamics of hematopoietic stem cells, which maintain long-term stemness and repopulating capacity at the population level through clonal succession.[41] Together with flow cytometry data, these findings highlight a lasting divergence in the differentiation programs of standard versus CAR T_{SCM} cells.

CAR T_{SCM} treatment failure depends on tumor- and host-related factors

CAR T cell expansion in peripheral blood correlates with clinical response.[24–27] Consistently, responders in the standard cohort exhibited significantly higher peak CAR T cell expansion compared with non-responders (median: 9.4 versus 1.2 CAR T cells/μL, respectively) (Figure 6A). In contrast, no significant differences in CAR T cell expansion were observed between responders and non-responders receiving CAR T_{SCM} cells (median: 26.9 versus 33.8 CAR T cells/μL, respectively) (Figure 6A). These findings emphasize the variability in T cell fitness among standard products, a key weakness that CAR T_{SCM} cells overcome, ensuring more robust and predictable engraftment. To investigate the mechanisms behind CAR T_{SCM} failure, we initially focused on the only patient (Pt #23) who experienced progressive disease (PD). Despite robust CAR T cell proliferation (Figures 6B and 6C) and preserved functionality (Figures 6D and 6E), as evidenced by the induction of B-cell aplasia, leukemia progressed undisturbed in both peripheral blood and BM (Figure 6D). Flow cytometry analysis of CD19 expression in pre- and post-CAR T BM biopsies revealed dim CD19 expression on pre-treatment leukemic blasts, which were enriched in the $CD19^{-}$ fraction following CAR T_{SCM} treatment (Figure 6E). These results indicate that leukemia progression was driven by insufficient CAR T cell reactivity against the low-density antigen on leukemic cells, as previously reported.[42] We further investigated another patient (Pt #30), the sole T_{SCM} recipient in whom CAR T cells failed to expand despite the infusion product being highly enriched (>80%) in T_{SCM} cells (Figure 6F). Therefore, we screened the patient's serum for the presence of multiple inhibitory cytokines within the first 3 days after CAR T cell infusion. While most of the tested cytokines remained within physiological levels in all T_{SCM}-treated patients, Pt #30 displayed strikingly elevated levels of IL-10 (Figure 6G). While recent studies have suggested that IL-10 may support T cell antitumor function in certain contexts,[43] our findings, albeit based on a single case, are more consistent with its well-established immunosuppressive role.[44] Emerging strategies such as dominant-negative IL-10 receptors, chimeric switch receptors, or synthetic intramembrane proteolysis receptors[45,46] may offer promising avenues to counteract IL-10-mediated immunosuppression in future CAR T_{SCM} cell-based therapies.

Humoral responses to the mouse-derived single-chain variable fragments (FMC63) included in the CD19-CAR construct have been previously reported.[31] Since CAR T cell infusion in our study was administered without lymphodepletion preconditioning, endogenous B cells likely retained the ability to mount humoral responses against FMC63, raising the possibility that anti-CAR antibodies (Abs) could hinder CAR T cell performance and clinical outcomes. We detected anti-CAR Abs in 35% of patients across the entire treatment cohorts (Figure 6H, left). Anti-CAR antibody levels correlated with the presence of B cells at the time of infusion (Figure 6H, right). To investigate the inhibitory potential of anti-CAR Abs on CAR T cell function, we assessed B cell aplasia as a surrogate marker of CAR T cell functionality in parallel with anti-CAR antibody detection in patients who received a second CAR T cell infusion. All four patients who underwent multiple CAR T cell treatments exhibited heightened humoral responses upon CAR re-exposure, underscoring a prime-boost effect (Figure S5). To assess the impact of anti-CAR Abs on CAR T cell functionality, we then focused on two patients who had detectable circulating B cells at the time of CAR T cell infusions (Figure 6I, left). Strikingly, while CAR T cells efficiently eliminated B cells following the first infusion, the second administration—even at higher doses—failed to reduce B cell numbers, coinciding with the induction of an anti-CAR response (Figure 6I, right). These findings provide compelling evidence that humoral responses can impair CAR T cell efficacy. Notably, Pt #25, who relapsed at 27 months and had no post-treatment biopsy to assess CD19 expression, showed the highest anti-CAR antibody levels (84 ng/mL) following CAR T cell infusion, suggesting a possible link between humoral inhibition of CAR T cell function and relapse. Although based on a limited number of cases, collectively our results suggest that CAR T_{SCM} treatment failure is primarily driven by tumor- and host-related factors—including low antigen density, immunosuppressive cytokines, and anti-CAR humoral responses—rather than intrinsic defects in T cell functionality and fitness.

DISCUSSION

CD19-directed CAR T cell therapies have transformed the treatment landscape for B-cell malignancies, achieving unprecedented complete remission rates in relapsed or refractory patients.[42,47,48] However, primary resistance and relapse remain significant challenges. A key factor limiting the efficacy of current CAR T cell therapies is the suboptimal fitness of certain cell products, which impairs their engraftment, expansion, and long-term persistence. Preclinical[10,11,15,49] and retrospective[7–9,14] studies have highlighted the importance of early memory T cells—particularly T_{SCM} cells—in determining therapeutic success. Despite this evidence, most CAR T cell products utilize unselected, heterogeneous preparations dominated by late-differentiated effector subsets. Recent clinical trials, however, have explored the use of less-differentiated CAR T cells, either by shortening manufacturing times,[50,51] employing cytokine cocktails that inhibit terminal differentiation,[52] or by selecting $CD62L^{+}$ T_N and T_{CM} cells as the starting population for manufacturing.[53–55] While the clinical outcomes in these studies have been promising, the absence of a benchmark control arm and the heterogeneity of the infused products hinder definitive conclusions regarding the contribution of specific T cell subsets to clinical response.

In this first-in-human trial, we employed a highly homogeneous $CD8^{+}$ CAR T cell product enriched for T_{SCM} cells and compared its performance with conventional CAR T cells.

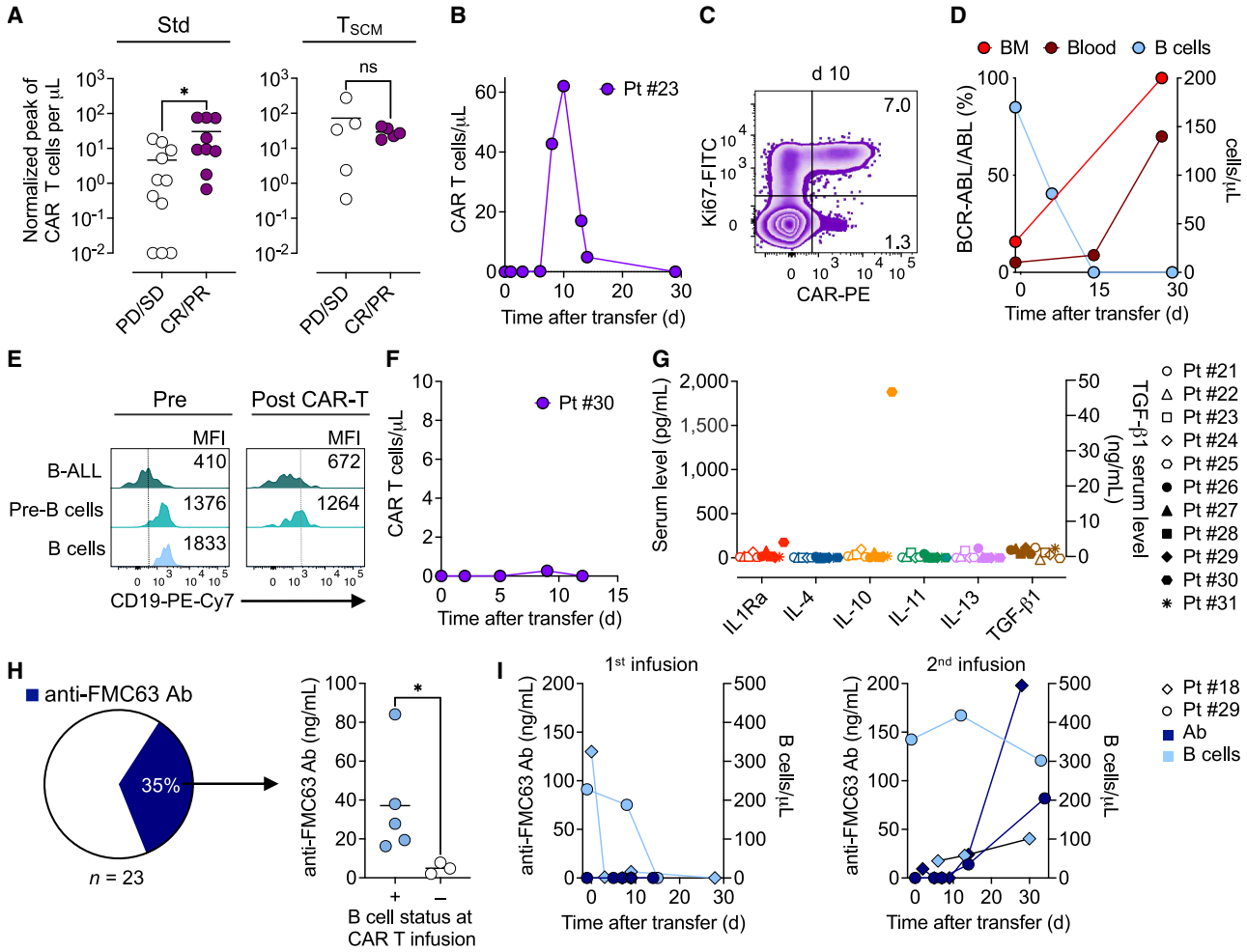

Figure 6. CAR T_{SCM} treatment failure depends on tumor- and host-related factors

(A) Correlation between best response and CAR T cell peak levels (assessed by qPCR) normalized to total infused dose (per 10^8 cells). Zero values plotted as 0.01 for log-scale visualization (*$p < 0.05$; ns, not significant, two-tailed Mann-Whitney test). PD, progressive disease; SD, stable disease; CR, complete response; and PR, partial response.

(B and C) CAR T cell expansion in a PD patient (Pt #23) after infusion of CAR T_{SCM} cells.

(B) Absolute CAR^+ T cell numbers per microliter of blood assessed by qPCR. Cells are normalized to the total infused dose (per 10^8 cells).

(C) Flow cytometry plot showing the frequency of proliferating CAR T cells at the peak of expansion as assessed by Ki67 staining. Numbers indicate the percentage of cells in each quadrant on the day of the peak.

(D) B cell counts and percent BCR-ABL transcript levels relative to ABL in bone marrow and blood in Pt #23 post-CAR T cell infusion.

(E) Flow cytometry plots showing CD19 expression levels on B-ALL, pre-B, and mature B cells in Pt #23 before and 1 month after CAR T cell infusion. Numbers in each plot represent CD19 mean fluorescence intensity (MFI). Dashed vertical line indicates the background levels of CD19 staining in $CD19^-$ cells.

(F) Absolute CAR T cell counts in Pt #30 from the T_{SCM} cohort. CAR levels were assessed by qPCR.

(G) Serum levels of immunosuppressive cytokines were detected in T_{SCM} recipients ($n = 11$) pre-CAR T cell infusion.

(H) Pie chart (left) showing the percentage of anti-FMC63 antibodies detected in the serum of standard and T_{SCM} recipients ($n = 23$) within the 30–90 days following the first CAR T cell infusion. Serum levels of anti-FMC63 antibodies versus detectable circulating B cells at the time of CAR T cell infusion (*$p < 0.05$; two-tailed Mann-Whitney test).

(I) Serum levels of anti-FMC63 antibodies and B cell count in two SD patients after the first and second CAR T cell infusion (standard, Pt #18; and T_{SCM}-enriched, Pt #29).

See also Figure S5.

Importantly, standard CAR T cells were engineered using the same CAR construct and administered to a comparable patient population at the same institution, serving as a reference in the absence of randomization. It is generally assumed that $CD4^+$ T cells are essential for effective CAR T cell therapy, given their role in supporting the generation of functional $CD8^+$ T cells during manufacturing[56] and contributing to the *in vivo* antitumor response.[57] This notion is largely based on studies in immunodeficient animal models,[57] which are inherently biased in favor of $CD4^+$ T cell function, as the lack of a functional immune system

amplifies their cytokine-mediated support. Evidence in humans is also circumstantial, as the detection of long-lived $CD4^+$ CAR T cells[58] is insufficient to establish their direct role in promoting tumor regression. Here, we provide evidence that $CD8^+$ CAR T_{SCM} cells alone can induce complete responses with greater efficiency than standard products containing $CD4^+$ T cells. Importantly, we showed that the $CD8^+$ T_{SCM} platform yields more reliable engraftment and expansion, thereby eliminating a major failure mode of current CAR T therapy.[59] As early expansion of CAR $CD8^+$ T cells correlates with clinical responses,[6,14] the use of $CD8^+$ T cell-enriched products may offer a therapeutic advantage. Additionally, the absence of $CD4^+$ T cells may confer benefits, such as an improved safety profile due to reduced CRS[32] and enhanced potency through the elimination of regulatory T cells, which are known to limit CAR T cell efficacy.[60]

Lymphodepletion—a standard-of-care approach—prior to CAR T cell therapy is regarded as essential for therapeutic success,[61] as it promotes the availability of homeostatic cytokines supporting T cell engraftment and function.[29,30] Challenging this paradigm, we observed robust CAR T cell expansion and potent antitumor responses following CAR T_{SCM} infusion, even without lymphodepleting chemotherapy. For doses above 1 million/kg, we observed an objective response rate of 71.4% (5 out of 7 patients), which is comparable with response rates reported for lymphodepleted patients treated with commercial CAR T cell products.[62] Strikingly, clinical responses were achieved with doses as low as 250,000 CAR T cells/kg (<20 million total cells). Notably, the T_{SCM} dose range and complete response rates were comparable with those reported in a recent trial employing IL-18-armored CD19-specific CAR T cells in lymphodepleted lymphoma patients,[51] underscoring the robust efficacy of T_{SCM} cells even without additional genetic enhancements or preconditioning strategies.

Beyond its clinical relevance, this study provides the opportunity to evaluate the function of $CD8^+$ CAR T_{SCM} cells in humans with exceptional resolution. We corroborated the distinct stem-like properties of this subset[10–12,63,64] by demonstrating their ability to generate effector progeny while reconstituting the T_{SCM} pool over time. Interestingly, longitudinal clonal tracking revealed that T_{SCM} maintenance was preferentially sustained at the population level through clonal succession rather than through self-renewal of individual clones. Similar clonal waves propelled by progenitor-exhausted T cells have been observed following checkpoint blockade,[65] reflecting a broader behavioral pattern of stem-like-driven immune responses. While it has traditionally been argued that stemness is maintained through asymmetric division at the single-cell level—producing one stem cell and one differentiating progeny—our findings, consistent with growing evidence,[41,66] suggest that this balance can also be achieved at the population level.

Although our findings were generated in the setting of relapse following allogeneic HSCT, the underlying biological principles are likely applicable beyond this context. In particular, the role of T_{SCM} cells in supporting CAR T cell expansion, persistence, and function may extend to autologous CAR T therapies and could play a critical role in overcoming current barriers in solid tumors, in which limited persistence and exhaustion have historically hindered efficacy.[67] In summary, this study demonstrates that a highly defined CAR T_{SCM} product represents a safe and effective platform, supporting its clinical potential and warranting further investigation for broader clinical application beyond the treatment of relapse post-alloHSCT.

Limitations of the study

As with any early-phase clinical trial, the relatively small patient cohort, the disease heterogeneity inherent to a basket trial design, and the absence of randomization limit the strength of clinical inferences that can be drawn. Thus, clinical comparisons should be considered exploratory and descriptive in nature, and the observed trends interpreted with caution until validated in larger, randomized studies. Additional aspects of the study may also have influenced the ability of CAR T_{SCM} cells to reach their full therapeutic potential. For example, the absence of lymphodepletion may have played a role by exacerbating the induction of humoral immune responses against the FMC63-CAR construct,[31,68] facilitating host T cell-mediated rejection of the allogeneic CAR T cells,[69] and limiting CAR T cell function[29] and expansion,[70] thereby constraining their durability and long-term activity. Furthermore, because the CAR T_{SCM} product was intentionally CD8-enriched, the absence of $CD4^+$ CAR T cells may have contributed to the late criss-crossing of EFS curves favoring standard products, potentially by limiting the ability to orchestrate endogenous immunity against $CD19^-$ tumor variants.[71] Unleashing the full therapeutic potential of CAR T_{SCM} cells will require studies conducted in lymphodepleted patients, the use of fully human or humanized CAR constructs,[72,73] and the potential inclusion of $CD4^+$ T cells to support durable immune responses.

RESOURCE AVAILABILITY

Lead contact

Further information and requests for resources and reagents should be directed to the lead contact, Luca Gattinoni (luca.gattinoni@lit.eu).

Materials availability

This study did not generate new unique reagents. Requests for research materials will be promptly reviewed by the National Cancer Institute and Leibniz Institute of Immunotherapy and will be released via a materials transfer agreement.

Data and code availability

The fastq files corresponding to the sequencing of IS amplicons generated for this study are deposited at European Genome-phenome Archive (EGA) under EGA: EGAS00001008119, EGAD00001015540. All other data supporting the findings of this study are available from the lead contact upon reasonable request.

ACKNOWLEDGMENTS

This research was supported by the NIH Intramural Research Program and the Deutsche Forschungsgemeinschaft (DFG, German Research Foundation) projektnummer 324392634-TRR 221, project A07. J.G.B. was supported by the Joachim Herz Foundation (add-on fellowship) and by the Fulbright Future Fellowship (Australian Fulbright Commission and The Kinghorn Foundation). E.L. is a CRI Lloyd J. Old STAR (CRI award 3914) and is supported by the Associazione Italiana per la Ricerca Sul Cancro (AIRC IG 2022 - ID 27391 and AIRC 5×1000 program UniCanVax 22757) and by EU funding within the MUR PNRR Italian Network of Excellence for advanced diagnosis (INNOVA, project no. PNC-E3-2022-23683266 PNC-HLS-DA). Sequencing was conducted at the NGS Unit of the Leibniz Institute of Immunotherapy (LIT),

Germany. We thank Hyunmi Halas for her assistance in retrieving CAR T cell infusion dose information. Special thanks to Johanna Raithel for her assistance with the integration site analysis and to Jaqueline Dirmeier and Niklas Wenzl from FACS-Analytics and Cell Sorting at LIT for their invaluable support with cell sorting. The graphical abstract and Figure 1A were created with BioRender.com.

AUTHOR CONTRIBUTIONS

J.N.K. is the principal investigator of the trial and the IND holder, and L.G. is the scientific principal investigator of the study. L.G., D.C.H., and J.N.K. conceived the project. L.G., G.I., L.B., E.L., and J.N.K. designed the experiments. L.G., G.I., A.S., S.P., D.S.-L., C.H.-L., J.G.B., J.F., Y.J., S. Gautam, C.S., A.M.-S., D.A.N., and N.P. performed the experiments. L.G., G.I., D.C.H., A.S., S.P., D.S.-L., D.A.N., N.S., R.C.S., N.P., M.R., S.A.R., L.B., E.L., J.N.B., and J.N.K. analyzed the data. L.G., G.I., J.N.K., and J.N.B. performed statistical analyses. L.G. and J.N.K. had unrestricted access to all data. J.M., S. Goff, L.M., J.C.Y., M.L.M.K., S.A.R., J.N.B., and J.N.K. provided patient care. S.L.H. and D.F.S. performed process development for cellular manufacturing and supervised cellular manufacturing. R.P. provided regulatory support. L.G., G.I., J.N.B., and J.N.K. wrote the manuscript. All authors agreed to submit the manuscript, read and approved the final draft, and take full responsibility for its content, including the accuracy of the data and the fidelity of the trial to the registered protocol and its statistical analysis. The contributions of the NIH author(s) are considered works of the United States government. The findings and conclusions presented in this paper are those of the author(s) and do not necessarily reflect the views of the NIH or the U.S. Department of Health and Human Services.

DECLARATION OF INTERESTS

L.G. and E.L. are inventors on a patent and receive royalties from Lyell Immunopharma related to methods for generating stem cell memory T (T_{SCM}) cells. L.G. has consulting agreements with Lyell Immunopharma and is a scientific advisor and stockholder of CellRep. S.G. is an employee of and holds stock in AstraZeneca. J.F. holds stocks in Lyell Immunopharma and Senti Biosciences. E.L. received consulting fees from Swarm Oncology, Menarini, Pfizer, BioLegend, and Amgen. J.N.K. has received research funding from Kite, a Gilead Company, and Bristol Myers Squibb. These funders did not support this work. J.N.K. has received royalties for CAR technology from Kite, a Gilead Company, Bristol Myers Squibb, and Kyverna.

STAR★METHODS

Detailed methods are provided in the online version of this paper and include the following:

- KEY RESOURCES TABLE
- EXPERIMENTAL MODEL AND STUDY PARTECIPANT DETAILS
  - Trial design and patient cohort
- METHOD DETAILS
  - Evaluation criteria of responses and toxicities
  - CAR-modified standard and T_{SCM}-$CD8^+$-enriched cell product manufacturing
  - Real-time qPCR for measuring blood CAR T cell absolute levels
  - Assessment of serum cytokine concentration
  - CAR T cell functionality evaluation by single-cell multiplex cytokine profiling
  - Polychromatic flow cytometry
  - CAR T cell longitudinal tracking via integration site analysis
  - Anti-CAR immune responses
- QUANTIFICATION AND STATISTICAL ANALYSIS
- ADDITIONAL RESOURCES

SUPPLEMENTAL INFORMATION

Supplemental information can be found online at https://doi.org/10.1016/j.cell.2026.03.047.

Received: August 27, 2025
Revised: November 3, 2025
Accepted: March 26, 2026

REFERENCES

1. D'Souza, A., Fretham, C., Lee, S.J., Arora, M., Brunner, J., Chhabra, S., Devine, S., Eapen, M., Hamadani, M., Hari, P., et al. (2020). Current Use of and Trends in Hematopoietic Cell Transplantation in the United States. Biol. Blood Marrow Transplant. *26*, e177–e182. https://doi.org/10.1016/j.bbmt.2020.04.013.
2. Roddie, C., and Peggs, K.S. (2011). Donor lymphocyte infusion following allogeneic hematopoietic stem cell transplantation. Expert Opin. Biol. Ther. *11*, 473–487. https://doi.org/10.1517/14712598.2011.554811.
3. Frey, N.V., and Porter, D.L. (2008). Graft-versus-host disease after donor leukocyte infusions: presentation and management. Best Pract. Res. Clin. Haematol. *21*, 205–222. https://doi.org/10.1016/j.beha.2008.02.007.
4. Smith, M., Zakrzewski, J., James, S., and Sadelain, M. (2018). Posttransplant chimeric antigen receptor therapy. Blood *131*, 1045–1052. https://doi.org/10.1182/blood-2017-08-752121.
5. Cruz, C.R.Y., Micklethwaite, K.P., Savoldo, B., Ramos, C.A., Lam, S., Ku, S., Diouf, O., Liu, E., Barrett, A.J., Ito, S., et al. (2013). Infusion of donor-derived CD19-redirected virus-specific T cells for B-cell malignancies relapsed after allogeneic stem cell transplant: a phase 1 study. Blood *122*, 2965–2973. https://doi.org/10.1182/blood-2013-06-506741.
6. Brudno, J.N., Somerville, R.P.T., Shi, V., Rose, J.J., Halverson, D.C., Fowler, D.H., Gea-Banacloche, J.C., Pavletic, S.Z., Hickstein, D.D., Lu, T.L., et al. (2016). Allogeneic T Cells That Express an Anti-CD19 Chimeric Antigen Receptor Induce Remissions of B-Cell Malignancies That Progress After Allogeneic Hematopoietic Stem-Cell Transplantation Without Causing Graft-Versus-Host Disease. J. Clin. Oncol. *34*, 1112–1121. https://doi.org/10.1200/JCO.2015.64.5929.
7. Fraietta, J.A., Lacey, S.F., Orlando, E.J., Pruteanu-Malinici, I., Gohil, M., Lundh, S., Boesteanu, A.C., Wang, Y., O'Connor, R.S., Hwang, W.T., et al. (2018). Determinants of response and resistance to CD19 chimeric antigen receptor (CAR) T cell therapy of chronic lymphocytic leukemia. Nat. Med. *24*, 563–571. https://doi.org/10.1038/s41591-018-0010-1.
8. Deng, Q., Han, G., Puebla-Osorio, N., Ma, M.C.J., Strati, P., Chasen, B., Dai, E., Dang, M., Jain, N., Yang, H., et al. (2020). Characteristics of anti-CD19 CAR T cell infusion products associated with efficacy and toxicity in patients with large B cell lymphomas. Nat. Med. *26*, 1878–1887. https://doi.org/10.1038/s41591-020-1061-7.
9. Bai, Z., Feng, B., McClory, S.E., de Oliveira, B.C., Diorio, C., Gregoire, C., Tao, B., Yang, L., Zhao, Z., Peng, L., et al. (2024). Single-cell CAR T atlas reveals type 2 function in 8-year leukaemia remission. Nature *634*, 702–711. https://doi.org/10.1038/s41586-024-07762-w.
10. Gattinoni, L., Zhong, X.S., Palmer, D.C., Ji, Y., Hinrichs, C.S., Yu, Z., Wrzesinski, C., Boni, A., Cassard, L., Garvin, L.M., et al. (2009). Wnt signaling arrests effector T cell differentiation and generates CD8+ memory stem cells. Nat. Med. *15*, 808–813. https://doi.org/10.1038/nm.1982.
11. Gattinoni, L., Lugli, E., Ji, Y., Pos, Z., Paulos, C.M., Quigley, M.F., Almeida, J.R., Gostick, E., Yu, Z., Carpenito, C., et al. (2011). A human memory T cell subset with stem cell-like properties. Nat. Med. *17*, 1290–1297. https://doi.org/10.1038/nm.2446.
12. Gattinoni, L., Speiser, D.E., Lichterfeld, M., and Bonini, C. (2017). T memory stem cells in health and disease. Nat. Med. *23*, 18–27. https://doi.org/10.1038/nm.4241.
13. Xu, Y., Zhang, M., Ramos, C.A., Durett, A., Liu, E., Dakhova, O., Liu, H., Creighton, C.J., Gee, A.P., Heslop, H.E., et al. (2014). Closely related T-memory stem cells correlate with in vivo expansion of CAR.CD19-T cells and are preserved by IL-7 and IL-15. Blood *123*, 3750–3759. https://doi.org/10.1182/blood-2014-01-552174.

14. Wang, Y., Tong, C., Lu, Y., Wu, Z., Guo, Y., Liu, Y., Wei, J., Wang, C., Yang, Q., and Han, W. (2023). Characteristics of premanufacture CD8(+)T cells determine CAR-T efficacy in patients with diffuse large B-cell lymphoma. Signal Transduct. Target. Ther. *8*, 409. https://doi.org/10.1038/s41392-023-01659-2.

15. Sabatino, M., Hu, J., Sommariva, M., Gautam, S., Fellowes, V., Hocker, J.D., Dougherty, S., Qin, H., Klebanoff, C.A., Fry, T.J., et al. (2016). Generation of clinical-grade CD19-specific CAR-modified CD8+ memory stem cells for the treatment of human B-cell malignancies. Blood *128*, 519–528. https://doi.org/10.1182/blood-2015-11-683847.

16. Better, M., Chiruvolu, V., Oliver, J., Lowe, E., Rossi, J.M., Perez, A., Navale, L., and Bot, A. (2016). 287. Production of KTE-C19 (Anti-CD19 CAR T Cells) for ZUMA-1: A Phase 1/2 Multi-Center Study Evaluating Safety and Efficacy in Subjects with Refractory Aggressive Non-Hodgkin Lymphoma (NHL). Mol. Ther. *24*, S115. https://doi.org/10.1016/S1525-0016(16)33096-9.

17. Cieri, N., Camisa, B., Cocchiarella, F., Forcato, M., Oliveira, G., Provasi, E., Bondanza, A., Bordignon, C., Peccatori, J., Ciceri, F., et al. (2013). IL-7 and IL-15 instruct the generation of human memory stem T cells from naive precursors. Blood *121*, 573–584. https://doi.org/10.1182/blood-2012-05-431718.

18. Hinrichs, C.S., Spolski, R., Paulos, C.M., Gattinoni, L., Kerstann, K.W., Palmer, D.C., Klebanoff, C.A., Rosenberg, S.A., Leonard, W.J., and Restifo, N.P. (2008). IL-2 and IL-21 confer opposing differentiation programs to CD8+ T cells for adoptive immunotherapy. Blood *111*, 5326–5333. https://doi.org/10.1182/blood-2007-09-113050.

19. Li, Y., Bleakley, M., and Yee, C. (2005). IL-21 influences the frequency, phenotype, and affinity of the antigen-specific CD8 T cell response. J. Immunol. *175*, 2261–2269. https://doi.org/10.4049/jimmunol.175.4.2261.

20. Ding, S., Wu, T.Y.H., Brinker, A., Peters, E.C., Hur, W., Gray, N.S., and Schultz, P.G. (2003). Synthetic small molecules that control stem cell fate. Proc. Natl. Acad. Sci. USA *100*, 7632–7637. https://doi.org/10.1073/pnas.0732087100.

21. Gattinoni, L., Klebanoff, C.A., and Restifo, N.P. (2012). Paths to stemness: building the ultimate antitumour T cell. Nat. Rev. Cancer *12*, 671–684. https://doi.org/10.1038/nrc3322.

22. Escobar, G., Mangani, D., and Anderson, A.C. (2020). T cell factor 1: A master regulator of the T cell response in disease. Sci. Immunol. *5*, eabb9726. https://doi.org/10.1126/sciimmunol.abb9726.

23. Puccio, S., Grillo, G., Alvisi, G., Scirgolea, C., Galletti, G., Mazza, E.M.C., Consiglio, A., De Simone, G., Licciulli, F., and Lugli, E. (2023). CRUSTY: a versatile web platform for the rapid analysis and visualization of high-dimensional flow cytometry data. Nat. Commun. *14*, 5102. https://doi.org/10.1038/s41467-023-40790-0.

24. Lee, D.W., Kochenderfer, J.N., Stetler-Stevenson, M., Cui, Y.K., Delbrook, C., Feldman, S.A., Fry, T.J., Orentas, R., Sabatino, M., Shah, N.N., et al. (2015). T cells expressing CD19 chimeric antigen receptors for acute lymphoblastic leukaemia in children and young adults: a phase 1 dose-escalation trial. Lancet *385*, 517–528. https://doi.org/10.1016/s0140-6736(14)61403-3.

25. Maude, S.L., Frey, N., Shaw, P.A., Aplenc, R., Barrett, D.M., Bunin, N.J., Chew, A., Gonzalez, V.E., Zheng, Z., Lacey, S.F., et al. (2014). Chimeric antigen receptor T cells for sustained remissions in leukemia. N. Engl. J. Med. *371*, 1507–1517. https://doi.org/10.1056/NEJMoa1407222.

26. Mueller, K.T., Maude, S.L., Porter, D.L., Frey, N., Wood, P., Han, X., Waldron, E., Chakraborty, A., Awasthi, R., Levine, B.L., et al. (2017). Cellular kinetics of CTL019 in relapsed/refractory B-cell acute lymphoblastic leukemia and chronic lymphocytic leukemia. Blood *130*, 2317–2325. https://doi.org/10.1182/blood-2017-06-786129.

27. Blumenberg, V., Busch, G., Baumann, S., Jitschin, R., Iacoboni, G., Gallur, L., Iraola-Truchuelo, J., Hoster, E., Winkelmann, M., Hellwig, K., et al. (2023). Early quantification of anti-CD19 CAR T cells by flow cytometry predicts response in R/R DLBCL. Blood Adv. *7*, 6844–6849. https://doi.org/10.1182/bloodadvances.2023010364.

28. Cao, G., Hu, Y., Pan, T., Tang, E., Asby, N., Althaus, T., Wan, J., Riedell, P.A., Bishop, M.R., Kline, J.P., et al. (2025). Two-stage CD8(+) CAR T-cell differentiation in patients with large B-cell lymphoma. Nat. Commun. *16*, 4205. https://doi.org/10.1038/s41467-025-59298-w.

29. Gattinoni, L., Finkelstein, S.E., Klebanoff, C.A., Antony, P.A., Palmer, D.C., Spiess, P.J., Hwang, L.N., Yu, Z., Wrzesinski, C., Heimann, D.M., et al. (2005). Removal of homeostatic cytokine sinks by lymphodepletion enhances the efficacy of adoptively transferred tumor-specific CD8+ T cells. J. Exp. Med. *202*, 907–912. https://doi.org/10.1084/jem.20050732.

30. Kochenderfer, J.N., Somerville, R.P.T., Lu, T., Shi, V., Bot, A., Rossi, J., Xue, A., Goff, S.L., Yang, J.C., Sherry, R.M., et al. (2017). Lymphoma Remissions Caused by Anti-CD19 Chimeric Antigen Receptor T Cells Are Associated With High Serum Interleukin-15 Levels. J. Clin. Oncol. *35*, 1803–1813. https://doi.org/10.1200/jco.2016.71.3024.

31. Turtle, C.J., Hanafi, L.A., Berger, C., Gooley, T.A., Cherian, S., Hudecek, M., Sommermeyer, D., Melville, K., Pender, B., Budiarto, T.M., et al. (2016). CD19 CAR-T cells of defined CD4+:CD8+ composition in adult B cell ALL patients. J. Clin. Investig. *126*, 2123–2138. https://doi.org/10.1172/jci85309.

32. Boulch, M., Cazaux, M., Cuffel, A., Ruggiu, M., Allain, V., Corre, B., Loe-Mie, Y., Hosten, B., Cisternino, S., Auvity, S., et al. (2023). A major role for CD4+ T cells in driving cytokine release syndrome during CAR T cell therapy. Cell Rep. Med. *4*, 101161. https://doi.org/10.1016/j.xcrm.2023.101161.

33. Bove, C., Arcangeli, S., Falcone, L., Camisa, B., El Khoury, R., Greco, B., De Lucia, A., Bergamini, A., Bondanza, A., Ciceri, F., et al. (2023). CD4 CAR-T cells targeting CD19 play a key role in exacerbating cytokine release syndrome, while maintaining long-term responses. J. Immunother. Cancer *11*, e005878. https://doi.org/10.1136/jitc-2022-005878.

34. Ho, M., Paruzzo, L., Noll, J.H., Stella, F., Devi, P., Ndeupen, S., Day, Y.A., Chen, G.M., Cohen, I.J., Ramirez-Fernandez, A., et al. (2026). CD4+ T cells mediate CAR-T cell-associated immune-related adverse events after BCMA CAR-T cell therapy. Nat. Med. *32*, 702–716. https://doi.org/10.1038/s41591-025-04121-8.

35. Norelli, M., Camisa, B., Barbiera, G., Falcone, L., Purevdorj, A., Genua, M., Sanvito, F., Ponzoni, M., Doglioni, C., Cristofori, P., et al. (2018). Monocyte-derived IL-1 and IL-6 are differentially required for cytokine-release syndrome and neurotoxicity due to CAR T cells. Nat. Med. *24*, 739–748. https://doi.org/10.1038/s41591-018-0036-4.

36. Giavridis, T., van der Stegen, S.J.C., Eyquem, J., Hamieh, M., Piersigilli, A., and Sadelain, M. (2018). CAR T cell-induced cytokine release syndrome is mediated by macrophages and abated by IL-1 blockade. Nat. Med. *24*, 731–738. https://doi.org/10.1038/s41591-018-0041-7.

37. Arcangeli, S., Bove, C., Mezzanotte, C., Camisa, B., Falcone, L., Manfredi, F., Bezzecchi, E., El Khoury, R., Norata, R., Sanvito, F., et al. (2022). CAR T cell manufacturing from naive/stem memory T lymphocytes enhances antitumor responses while curtailing cytokine release syndrome. J. Clin. Investig. *132*, e150807. https://doi.org/10.1172/jci150807.

38. Rossi, J., Paczkowski, P., Shen, Y.W., Morse, K., Flynn, B., Kaiser, A., Ng, C., Gallatin, K., Cain, T., Fan, R., et al. (2018). Preinfusion polyfunctional anti-CD19 chimeric antigen receptor T cells are associated with clinical outcomes in NHL. Blood *132*, 804–814. https://doi.org/10.1182/blood-2018-01-828343.

39. Street, K., Risso, D., Fletcher, R.B., Das, D., Ngai, J., Yosef, N., Purdom, E., and Dudoit, S. (2018). Slingshot: cell lineage and pseudotime inference for single-cell transcriptomics. BMC Genomics *19*, 477. https://doi.org/10.1186/s12864-018-4772-0.

40. Setty, M., Tadmor, M.D., Reich-Zeliger, S., Angel, O., Salame, T.M., Kathail, P., Choi, K., Bendall, S., Friedman, N., and Pe'er, D. (2016).

Wishbone identifies bifurcating developmental trajectories from single-cell data. Nat. Biotechnol. *34*, 637–645. https://doi.org/10.1038/nbt.3569.

41. Kim, S., Kim, N., Presson, A.P., Metzger, M.E., Bonifacino, A.C., Sehl, M., Chow, S.A., Crooks, G.M., Dunbar, C.E., An, D.S., et al. (2014). Dynamics of HSPC repopulation in nonhuman primates revealed by a decade-long clonal-tracking study. Cell Stem Cell *14*, 473–485. https://doi.org/10.1016/j.stem.2013.12.012.
42. Spiegel, J.Y., Patel, S., Muffly, L., Hossain, N.M., Oak, J., Baird, J.H., Frank, M.J., Shiraz, P., Sahaf, B., Craig, J., et al. (2021). CAR T cells with dual targeting of CD19 and CD22 in adult patients with recurrent or refractory B cell malignancies: a phase 1 trial. Nat. Med. *27*, 1419–1431. https://doi.org/10.1038/s41591-021-01436-0.
43. Zhao, Y., Chen, J., Andreatta, M., Feng, B., Xie, Y.-Q., Wenes, M., Wang, Y., Gao, M., Hu, X., Romero, P., et al. (2024). IL-10-expressing CAR T cells resist dysfunction and mediate durable clearance of solid tumors and metastases. Nat. Biotechnol. *42*, 1693–1704. https://doi.org/10.1038/s41587-023-02060-8.
44. de Waal Malefyt, R., Abrams, J., Bennett, B., Figdor, C.G., and de Vries, J.E. (1991). Interleukin 10(IL-10) inhibits cytokine synthesis by human monocytes: an autoregulatory role of IL-10 produced by monocytes. J. Exp. Med. *174*, 1209–1220. https://doi.org/10.1084/jem.174.5.1209.
45. Rafiq, S., Hackett, C.S., and Brentjens, R.J. (2020). Engineering strategies to overcome the current roadblocks in CAR T cell therapy. Nat. Rev. Clin. Oncol. *17*, 147–167. https://doi.org/10.1038/s41571-019-0297-y.
46. Piraner, D.I., Abedi, M.H., Duran Gonzalez, M.J., Chazin-Gray, A., Lin, A., Zhu, I., Ravindran, P.T., Schlichthaerle, T., Huang, B., Bearchild, T.H., et al. (2025). Engineered receptors for soluble cellular communication and disease sensing. Nature *638*, 805–813. https://doi.org/10.1038/s41586-024-08366-0.
47. Westin, J.R., Oluwole, O.O., Kersten, M.J., Miklos, D.B., Perales, M.A., Ghobadi, A., Rapoport, A.P., Sureda, A., Jacobson, C.A., Farooq, U., et al. (2023). Survival with Axicabtagene Ciloleucel in Large B-Cell Lymphoma. N. Engl. J. Med. *389*, 148–157. https://doi.org/10.1056/NEJMoa2301665.
48. Siddiqi, T., Maloney, D.G., Kenderian, S.S., Brander, D.M., Dorritie, K., Soumerai, J., Riedell, P.A., Shah, N.N., Nath, R., Fakhri, B., et al. (2023). Lisocabtagene maraleucel in chronic lymphocytic leukaemia and small lymphocytic lymphoma (TRANSCEND CLL 004): a multicentre, open-label, single-arm, phase 1–2 study. Lancet *402*, 641–654. https://doi.org/10.1016/s0140-6736(23)01052-8.
49. Galletti, G., De Simone, G., Mazza, E.M.C., Puccio, S., Mezzanotte, C., Bi, T.M., Davydov, A.N., Metsger, M., Scamardella, E., Alvisi, G., et al. (2020). Two subsets of stem-like CD8+ memory T cell progenitors with distinct fate commitments in humans. Nat. Immunol. *21*, 1552–1562. https://doi.org/10.1038/s41590-020-0791-5.
50. Dickinson, M.J., Barba, P., Jäger, U., Shah, N.N., Blaise, D., Briones, J., Shune, L., Boissel, N., Bondanza, A., Mariconti, L., et al. (2023). A Novel Autologous CAR-T Therapy, YTB323, with Preserved T-cell Stemness Shows Enhanced CAR T-cell Efficacy in Preclinical and Early Clinical Development. Cancer Discov. *13*, 1982–1997. https://doi.org/10.1158/2159-8290.Cd-22-1276.
51. Svoboda, J., Landsburg, D.J., Gerson, J., Nasta, S.D., Barta, S.K., Chong, E.A., Cook, M., Frey, N.V., Shea, J., Cervini, A., et al. (2025). Enhanced CAR T-Cell Therapy for Lymphoma after Previous Failure. N. Engl. J. Med. *392*, 1824–1835. https://doi.org/10.1056/NEJMoa2408771.
52. Caballero, A.C., Ujaldón-Miró, C., Pujol-Fernández, P., Montserrat-Torres, R., Guardiola-Perello, M., Escudero-López, E., Garcia-Cadenas, I., Esquirol, A., Martino, R., Jara-Bustamante, P., et al. (2025). HSP-CAR30 with a high proportion of less-differentiated T cells promotes durable responses in refractory CD30+ lymphoma. Blood *145*, 1788–1801. https://doi.org/10.1182/blood.2024026758.
53. Larson, S.M., Walthers, C.M., Ji, B., Ghafouri, S.N., Naparstek, J., Trent, J., Chen, J.M., Roshandell, M., Harris, C., Khericha, M., et al. (2023). CD19/CD20 Bispecific Chimeric Antigen Receptor (CAR) in Naive/Memory T Cells for the Treatment of Relapsed or Refractory Non-Hodgkin Lymphoma. Cancer Discov. *13*, 580–597. https://doi.org/10.1158/2159-8290.Cd-22-0964.
54. Aldoss, I., Khaled, S.K., Wang, X., Palmer, J., Wang, Y., Wagner, J.R., Clark, M.C., Simpson, J., Paul, J., Vyas, V., et al. (2023). Favorable Activity and Safety Profile of Memory-Enriched CD19-Targeted Chimeric Antigen Receptor T-Cell Therapy in Adults with High-Risk Relapsed/Refractory ALL. Clin. Cancer Res. *29*, 742–753. https://doi.org/10.1158/1078-0432.Ccr-22-2038.
55. Brown, C.E., Hibbard, J.C., Alizadeh, D., Blanchard, M.S., Natri, H.M., Wang, D., Ostberg, J.R., Aguilar, B., Wagner, J.R., Paul, J.A., et al. (2024). Locoregional delivery of IL-13Rα2-targeting CAR-T cells in recurrent high-grade glioma: a phase 1 trial. Nat. Med. *30*, 1001–1012. https://doi.org/10.1038/s41591-024-02875-1.
56. Lee, S.Y., Lee, D.H., Sun, W., Cervantes-Contreras, F., Basom, R.S., Wu, F., Liu, S., Rai, R., Mirzaei, H.R., O'Steen, S., et al. (2023). CD8(+) chimeric antigen receptor T cells manufactured in absence of CD4(+) cells exhibit hypofunctional phenotype. J. Immunother. Cancer *11*, e007803. https://doi.org/10.1136/jitc-2023-007803.
57. Sommermeyer, D., Hudecek, M., Kosasih, P.L., Gogishvili, T., Maloney, D.G., Turtle, C.J., and Riddell, S.R. (2016). Chimeric antigen receptor-modified T cells derived from defined CD8+ and CD4+ subsets confer superior antitumor reactivity in vivo. Leukemia *30*, 492–500. https://doi.org/10.1038/leu.2015.247.
58. Melenhorst, J.J., Chen, G.M., Wang, M., Porter, D.L., Chen, C., Collins, M.A., Gao, P., Bandyopadhyay, S., Sun, H., Zhao, Z., et al. (2022). Decade-long leukaemia remissions with persistence of CD4+ CAR T cells. Nature *602*, 503–509. https://doi.org/10.1038/s41586-021-04390-6.
59. Shah, N.N., and Fry, T.J. (2019). Mechanisms of resistance to CAR T cell therapy. Nat. Rev. Clin. Oncol. *16*, 372–385. https://doi.org/10.1038/s41571-019-0184-6.
60. Good, Z., Spiegel, J.Y., Sahaf, B., Malipatlolla, M.B., Ehlinger, Z.J., Kurra, S., Desai, M.H., Reynolds, W.D., Wong Lin, A., Vandris, P., et al. (2022). Post-infusion CAR Treg cells identify patients resistant to CD19-CAR therapy. Nat. Med. *28*, 1860–1871. https://doi.org/10.1038/s41591-022-01960-7.
61. Casucci, M., and Ciceri, F. (2021). A second CD19 CAR T-cell infusion: yes or no? Blood *137*, 284–286. https://doi.org/10.1182/blood.2020009206.
62. Arunachalam, A.K., Grégoire, C., Coutinho de Oliveira, B., and Melenhorst, J.J. (2024). Advancing CAR T-cell therapies: Preclinical insights and clinical translation for hematological malignancies. Blood Rev. *68*, 101241. https://doi.org/10.1016/j.blre.2024.101241.
63. Biasco, L., Izotova, N., Rivat, C., Ghorashian, S., Richardson, R., Guvenel, A., Hough, R., Wynn, R., Popova, B., Lopes, A., et al. (2021). Clonal expansion of T memory stem cells determines early anti-leukemic responses and long-term CAR T cell persistence in patients. Nat. Cancer *2*, 629–642. https://doi.org/10.1038/s43018-021-00207-7.
64. Oliveira, G., Ruggiero, E., Stanghellini, M.T.L., Cieri, N., D'Agostino, M., Fronza, R., Lulay, C., Dionisio, F., Mastaglio, S., Greco, R., et al. (2015). Tracking genetically engineered lymphocytes long-term reveals the dynamics of T cell immunological memory. Sci. Transl. Med. *7*, 317ra198. https://doi.org/10.1126/scitranslmed.aac8265.
65. Wang, K., Coutifaris, P., Brocks, D., Wang, G., Azar, T., Solis, S., Nandi, A., Anderson, S., Han, N., Manne, S., et al. (2024). Combination anti-PD-1 and anti-CTLA-4 therapy generates waves of clonal responses that include progenitor-exhausted CD8+ T cells. Cancer Cell *42*, 1582–1597.e10. https://doi.org/10.1016/j.ccell.2024.08.007.
66. Simons, B.D., and Clevers, H. (2011). Strategies for homeostatic stem cell self-renewal in adult tissues. Cell *145*, 851–862. https://doi.org/10.1016/j.cell.2011.05.033.
67. Chan, J.D., Lai, J., Slaney, C.Y., Kallies, A., Beavis, P.A., and Darcy, P.K. (2021). Cellular networks controlling T cell persistence in adoptive cell

therapy. Nat. Rev. Immunol. *21*, 769–784. https://doi.org/10.1038/s41577-021-00539-6.

68. Awasthi, R., Pacaud, L., Waldron, E., Tam, C.S., Jäger, U., Borchmann, P., Jaglowski, S., Foley, S.R., van Besien, K., Wagner-Johnston, N.D., et al. (2020). Tisagenlecleucel cellular kinetics, dose, and immunogenicity in relation to clinical factors in relapsed/refractory DLBCL. Blood Adv. *4*, 560–572. https://doi.org/10.1182/bloodadvances.2019000525.

69. Perica, K., Kotchetkov, I.S., Mansilla-Soto, J., Ehrich, F., Herrera, K., Shi, Y., Dobrin, A., Gönen, M., and Sadelain, M. (2025). HIV immune evasin Nef enhances allogeneic CAR T cell potency. Nature *640*, 793–801. https://doi.org/10.1038/s41586-025-08657-0.

70. Cieri, N., Oliveira, G., Greco, R., Forcato, M., Taccioli, C., Cianciotti, B., Valtolina, V., Noviello, M., Vago, L., Bondanza, A., et al. (2015). Generation of human memory stem T cells after haploidentical T-replete hematopoietic stem cell transplantation. Blood *125*, 2865–2874. https://doi.org/10.1182/blood-2014-11-608539.

71. Cheloni, G., Karagkouni, D., Pita-Juarez, Y., Torres, D., Kanata, E., Liegel, J., Avigan, Z., Saldarriaga, I., Chedid, G., Rallis, K., et al. (2025). Durable response to CAR T is associated with elevated activation and clonotypic expansion of the cytotoxic native T cell repertoire. Nat. Commun. *16*, 4819. https://doi.org/10.1038/s41467-025-59904-x.

72. Brudno, J.N., Lam, N., Vanasse, D., Shen, Y.W., Rose, J.J., Rossi, J., Xue, A., Bot, A., Scholler, N., Mikkilineni, L., et al. (2020). Safety and feasibility of anti-CD19 CAR T cells with fully human binding domains in patients with B-cell lymphoma. Nat. Med. *26*, 270–280. https://doi.org/10.1038/s41591-019-0737-3.

73. Gauthier, J., Liang, E.C., Huang, J.J., Kimble, E.L., Hirayama, A.V., Fiorenza, S., Voutsinas, J.M., Wu, Q.V., Jaeger-Ruckstuhl, C.A., Pender, B.S., et al. (2025). Phase 1 study of CD19 CAR T-cell therapy harboring a fully human scFv in CAR-naïve adult patients with B-ALL. Blood Adv. *9*, 1861–1872. https://doi.org/10.1182/bloodadvances.2024015314.

74. Przepiorka, D., Weisdorf, D., Martin, P., Klingemann, H.G., Beatty, P., Hows, J., and Thomas, E.D. (1995). Consensus Conference on Acute GVHD Grading. Bone Marrow Transplant. *15*, 825–828.

75. Filipovich, A.H., Weisdorf, D., Pavletic, S., Socie, G., Wingard, J.R., Lee, S.J., Martin, P., Chien, J., Przepiorka, D., Couriel, D., et al. (2005). National Institutes of Health Consensus Development Project on Criteria for Clinical Trials in Chronic Graft-versus-Host Disease: I. Diagnosis and Staging Working Group Report. Biol. Blood Marrow Transplant. *11*, 945–956. https://doi.org/10.1016/j.bbmt.2005.09.004.

76. Cheson, B.D., Pfistner, B., Juweid, M.E., Gascoyne, R.D., Specht, L., Horning, S.J., Coiffier, B., Fisher, R.I., Hagenbeek, A., Zucca, E., et al. (2007). Revised response criteria for malignant lymphoma. J. Clin. Oncol. *25*, 579–586. https://doi.org/10.1200/jco.2006.09.2403.

77. Cheson, B.D., Fisher, R.I., Barrington, S.F., Cavalli, F., Schwartz, L.H., Zucca, E., Lister, T.A., et al.; Alliance, Australasian Leukaemia and Lymphoma Group, Eastern Cooperative Oncology Group, European Mantle Cell Lymphoma Consortium (2014). Recommendations for initial evaluation, staging, and response assessment of Hodgkin and non-Hodgkin lymphoma: the Lugano classification. J. Clin. Oncol. *32*, 3059–3068. https://doi.org/10.1200/jco.2013.54.8800.

78. Hallek, M., Cheson, B.D., Catovsky, D., Caligaris-Cappio, F., Dighiero, G., Döhner, H., Hillmen, P., Keating, M., Montserrat, E., Chiorazzi, N., et al. (2018). iwCLL guidelines for diagnosis, indications for treatment, response assessment, and supportive management of CLL. Blood *131*, 2745–2760. https://doi.org/10.1182/blood-2017-09-806398.

79. Lee, D.W., Santomasso, B.D., Locke, F.L., Ghobadi, A., Turtle, C.J., Brudno, J.N., Maus, M.V., Park, J.H., Mead, E., Pavletic, S., et al. (2019). ASTCT Consensus Grading for Cytokine Release Syndrome and Neurologic Toxicity Associated with Immune Effector Cells. Biol. Blood Marrow Transplant. *25*, 625–638. https://doi.org/10.1016/j.bbmt.2018.12.758.

80. Yan, A., Baricordi, C., Nguyen, Q., Barbarossa, L., Loperfido, M., and Biasco, L. (2023). IS-Seq: a bioinformatics pipeline for integration sites analysis with comprehensive abundance quantification methods. BMC Bioinform. *24*, 286. https://doi.org/10.1186/s12859-023-05390-1.

Please cite this article in press as: Gattinoni et al., Distinct *in vivo* dynamics of donor-derived stem cell memory CAR T cells post-allogeneic HSCT relapse, Cell (2026), https://doi.org/10.1016/j.cell.2026.03.047

STAR★METHODS

KEY RESOURCES TABLE

REAGENT or RESOURCE	SOURCE	IDENTIFIER
Antibodies		
eBioscience™ Foxp3/Transcription Factor Staining Buffer	Invitrogen	00-5523-00
hTIGIT PerCP-eF710	eBioscience	Cat#: 46-9500-42: RRID: AB_10853679
hKi67 FITC	BD	Cat#: 556026 (51-35404X) B56; RRID:AB_396302
hCD29 APC-Cy7	BioLegend	Cat#: 303014; RRID: AB_493580
hGranzyme B AF700	BD	Cat#: 560213; RRID: AB_1645453
hGranzyme K AF647	Santa Cruz	Cat#: sc-56125; RRID: AB_2263772
hCD28 BV786	BioLegend	Cat#: 302950; RRID: AB_2632607
hCD38 BV711	BioLegend	Cat#: 303528 ; RRID: AB_2563811
anti-hCD134 (OX40) BV650	BD	Cat#: 563658 : RRID: AB_2738353
hCD57 BV605	BD	Cat#: 624290; RRID: AB_3683745
hCD45RO BV570	BioLegend	Cat#: 304226;RRID: AB_2563818
hPD1 (CD279) BV480	BD	Cat#: 566112; RRID: AB_2739514
hCD8 BUV805	BD	Cat#: 564912; RRID: AB_2744465
hCD95 BUV737	BD	Cat#: 564710; RRID: AB_2738907
hHLA-DR BUV661	BD	Cat#: 565073; RRID: AB_2722500
hCD4 BUV615	BD	Cat#: 624297; RRID: AB_2875044
hCD25 BUV563	BD	Cat#: 565699: RRID: AB_2744341
hCD3 BUV496	BD	Cat#: 612940; RRID: AB_2870222
CD45RA BUV395	BD	Cat#: 740315; RRID: AB_2740052
hT-bet PE-Cy7	eBioscience	Cat#: BMS25-5825-82; RRID: AB_11042699
hFoxP3 PECy5.5	eBioscience	Cat#: 35-4776-42; RRID: AB_11218094
hCD127 PE-Cy5	eBioscience	Cat#: 15-1278-42; RRID: AB_2043801
hCD197 (CCR7) PE-CF594	BD	Cat#: 562381;RRID: AB_11153301
hCD19 BV570	BioLegend	Cat#: 302236; RRID: AB_2563606
hCD45 BUV395	BD	Cat#: 563792; RRID: AB_2869519
hCD16 PE-Cy7	BD	Cat#: 557744;RRID: AB_396850
hCD56 PE-CF594	BD	Cat#: 562289;RRID: AB_11152080
hHLA-DR BUV661	BD	Cat#: 565073; RRID: AB_2722500
CD159a (NKG2A) VioBright FITC	Miltenyi	Cat#: 130-113-568; RRID: AB_2726173
hCD11c APC	BD	Cat#: 559877; RRID: AB_398680
hCD14 BV510	BioLegend	Cat#: 301842; RRID: AB_2561946
hCD57 BV605	BD	Cat#: 624290; RRID: AB_3683745
NKG2C BV650	BD	Cat#: 748165; RRID: AB_2872626
Hcd3 BUV496	BD	Cat#: 612940; RRID: AB_2870222
hGranzyme B AF700	BD	Cat#: 560213; RRID: AB_1645453
anti-FMC63 PE	AcroBiosystem	Cat#: FM3-HPY53; RRID: AB_2921284
Bacterial and virus strains		
MSGV FMC63-28 gamma retrovirus	Brudno et al.[6]	N/A
Biological samples		
Healthy donor PBMCs	National Institute of Health	NCT01087294

(*Continued on next page*)

Please cite this article in press as: Gattinoni et al., Distinct *in vivo* dynamics of donor-derived stem cell memory CAR T cells post-allogeneic HSCT relapse, Cell (2026), https://doi.org/10.1016/j.cell.2026.03.047

Continued

REAGENT or RESOURCE	SOURCE	IDENTIFIER
Patient PBCMs	National Institute of Health	NCT01087294
Patient Serums	National Institute of Health	NCT01087294
Patient plasma	National Institute of Health	NCT01087294
Chemicals, peptides, and recombinant proteins		
Guanidine Hydrochloride	Sigma	Cat# G3272-500G
Critical commercial assays		
Anti-CD19 (FMC63) CAR Immunogenicity ELISA KIT	AcroBiosystem	RAB-P001
HCYTA-60K-01 Human Cyto Panel A	Merck	HCYTA-60K-01
MILLIPLEX TGF-beta 1,2,3 MAGNETIC Bead Kit	Merck	R-7658020.3
CD235a (Glycophorin A) MicroBeads, human	Miltenyi	130-050-501
Human Cytokine/Chemokine/Growth Factor Panel A 38 Plex Kit	Merck	HCYTA-60K-PX38
MILLIPLEX Human High Sensitivity T Cell Magnetic Bead 13 Plex PREMIXED Kit	Merck	HSTCMAG28SPMX13
MILLIPLEX Human High Sensitivity T Cell 21 Plex PREMIXED Magnetic Bead Kit	Merck	HT17MG-14K-PX25
Single-Cell Secretome Adaptive Immune Chips – 8 (Human)	IsoPlexis	ISOCODE-1001-8
PCR Master mix	ThermoFisher	K0172
NEBNext® Ultra™ II Ligation Module	New England Biolabs	E7595S
NEBNext® Ultra™ II End Repair/dA-Tailing Module	New England Biolabs	E7546S
REPLI-g Mini kit	QIAGEN	150023
Deposited data		
Integration site analysis data	This paper	EGA study ID: EGAS00001008119 DatasetID: EGAD00001015540
Experimental models: Cell lines		
Human CD19^{+} K562 cell lines	Laboratory of Luca Gattinoni	N/A
Oligonucleotides		
RV_LTR1 1st PCR: 5′-TGT TCC TAA CCT TGA TCT GAA CTT-3′	This Paper	N/A
LCP1 1st PCR: 5′-GAC CCG GGA GAT CTG AAT TC-3′	This Paper	N/A
RV_LTR2 2nd PCR: 5′-TTC CAT GCC TTG CAA AAT GGC-3′	This Paper	N/A
LCP2 2nd PCR: 5′-GAT CTG AAT TCA GTG GCA CAG-3′	This Paper	N/A
LC TA Sonic Sense Duplex: 5′-GAC CCG GGA GAT CTG AAT TCA GTG GCA CAG CAG TTA GGN NNN NNG TAA GGN NNN NNA GAT CTG GAA TGA ACT GGC C-3′ 3′-/3AmMO/-TCT AGA CCT TAC TTG ACC GGT-5′	This Paper	N/A
FMC63CAR (Taqman): Forward ACAGGCTCCACCTCTGGAT Reverse: GTTTCCCTCGCCCTTGGT Probe: TCCCTCGCCAGATCC	This paper	N/A

(*Continued on next page*)

Continued

REAGENT or RESOURCE	SOURCE	IDENTIFIER
Recombinant DNA		
pCMV6-AC beta actin plasmid	Origene	SC319328
Software and algorithms		
xPONENT 4.2 software	Luminex MAGPIX	https://www.rndsystems.com/products/luminex-magpix-instrument-with-xponent-43_magpix-xpon42
SparkControl	Tecan Spark 10M i	Tecan website
FlowJo (v10.10.0)	BD	https://flowjo.com/flowjo10/download
Prism software v10.2.3	GraphPad	https://www.graphpad.com/updates/prism-10-2-3-release-notes
Other		
Sequencing data were processed with Cell Ranger (v7.1.0)	This Paper	N/A
Next-generation sequencing was performed on the Illumina NextSeq 2000	Illumina	20038897
QuantStudio™ 3 Real-Time PCR System	ThermoFisher	ThermoFisher

EXPERIMENTAL MODEL AND STUDY PARTECIPANT DETAILS

Trial design and patient cohort

A single-center, Phase 1 dose-escalation trial of donor-derived anti-CD19 CAR T cells for patients with relapsed or refractory B-cell malignancies following human leukocyte antigen (HLA)-matched alloHSCT was conducted as previously reported (NCT01087294).[6] After the initial 20 patients were treated with the conventional cell culture process, the trial protocol was amended to allow treatment of a second cohort of patients, who received $CD8^+$ T_{SCM}-enriched CAR T cells on a separate dose-escalation (Table S1). Primary objectives were to assess safety, tolerability and to identify a maximally tolerated and/or recommended Phase 2 dose of CAR T_{SCM} cells. Secondary objectives included evaluating CAR T_{SCM} cell anti-tumor efficacy and persistence. Patients aged 18–75 years with $CD19^+$ B-cell malignancies with measurable malignancy after a prior $\geq$ 9/10 HLA-matched sibling or unrelated donor alloHSCT were eligible to participate. A prior DLI was not required for eligibility for the T_{SCM} cohort. Minimal or no evidence of acute or chronic GvHD, no receipt of systemic immunosuppression for $\geq$ 28 days, an Eastern Cooperative Oncology Group (ECOG) performance status of $\leq$ 2, and essentially normal organ function were required for eligibility. The characteristics and clinical course of the 20 patients who received the standard CAR T cells are summarized in Table S2. Characteristics of the 11 patients who received CAR T_{SCM} cells are summarized in Table S1. Three of these patients self-identified as female; 8 of these patients identified as male. Patients had received a median of 2 prior lines of therapy after the most recent alloHSCT (range 0–8). Patients' prior post-transplant therapies are summarized in Table S6.

PBMCs were collected from each patient's transplant donor by leukapheresis. Patients received a single infusion of CAR T_{SCM} cells with no preconditioning chemotherapy. Second infusions were allowed for patients with a partial response (PR), stable disease (SD), or relapse after complete response (CR) and persistent CD19 expression on the malignancy. The clinical trial was approved by the National Institutes of Health Institutional Review Board. All patients and matched donors provided written informed consent prior to enrollment in compliance with the Declaration of Helsinki.

METHOD DETAILS

Evaluation criteria of responses and toxicities

Minimal acute GvHD was defined as grade 0-I,[74] and minimal chronic GvHD was defined as chronic GvHD with no organ site exceeding a score of 1, except for the skin, for which a score of 1 or 2 was allowed.[75] Malignancy responses were assessed using published criteria for non-Hodgkin lymphoma[76,77] and chronic lymphocytic leukemia.[78] Criteria for CR of B-cell acute lymphoblastic leukemia were as previously described.[6] CRS was graded per the ASTCT criteria.[79] Other adverse events, including ICANS, were graded according to the Common Terminology Criteria for Adverse Events version 4.03.

CAR-modified standard and T_{SCM}-$CD8^+$-enriched cell product manufacturing

Analogous to axicabtagene ciloleucel,[16] standard CAR T cells were transduced with the same CAR construct and generated by activating donor-derived PBMCs with soluble anti-CD3 and IL-2, as previously described.[6] Two days after activation, PBMCs were transduced in six-well plates pre-coated with Retronectin™ and anti-CD19 CAR gammaretroviral vector. CAR-modified

$CD8^+$ T_{SCM}-enriched cells were prepared from PBMCs obtained from each patient's transplant donor leukapheresis. $CD8^+CD62L^+CD45RA^+$ T cells were serially enriched using Fab-Streptamer™ technology and stimulated with CD3/CD28 microbeads in media supplemented with IL-7, IL-21, and the GSK-3β inhibitor TWS119, as previously described[15]. T cells were subsequently transduced with the same anti-CD19 CAR gammaretroviral vector and infused into patients after 7 days of culture.

Real-time qPCR for measuring blood CAR T cell absolute levels

Circulating CAR T cells were quantified up to 36 days post-infusion by qPCR targeting the integrated FMC63 CAR transgene. Genomic DNA from pre- and post-infusion samples was extracted and amplified in duplicate using CAR-specific primers and TaqMan probes, as previously described.[6] The percentage of CAR^+ T cells in infusion products was determined by flow cytometry using an anti-FMC63 antibody. Post-infusion CAR T cell frequencies were calculated by comparison to the patient-specific standard curve and normalized to β-actin. Absolute circulating CAR T cell counts were derived by multiplying the CAR^+ T cell percentage by the sum of absolute lymphocyte and monocyte counts, expressed as CAR^+ T cells/μL of peripheral blood.[6] All values were normalized to the total infused CAR T cell dose.

Assessment of serum cytokine concentration

Cryopreserved serum samples collected pre- and post-CAR T cell infusion were thawed and analyzed for cytokine levels using the MilliPlex Human High Sensitivity T Cell Magnetic Bead Panel and the MILLIPLEX Human Cytokine/Chemokine/Growth Factor Panel kits, following the manufacturer's protocols. Cytokines were detected using the Luminex MAGPIX system with xPONENT 4.2 software. Median Fluorescence Intensity values were processed using the 5-parameter logistic regression method in Belysa software.

CAR T cell functionality evaluation by single-cell multiplex cytokine profiling

Cryopreserved CAR T cell infusion products were thawed and cultured overnight in complete AIMV medium supplemented with 5% FBS, penicillin (100 U/mL), streptomycin (100 μg/mL), GlutaMAX (2 mM), and HEPES (10 mM). Standard CAR T cells were supplemented with IL-2 (250 IU/mL) while CAR T_{SCM} cells were supplemented with IL-7 (5 ng/mL) and IL-21 (30 ng/mL). After recovery, cells were stained with Pacific Blue anti-CD8, APC anti-CD19 CAR antibodies, and 7-AAD, and viable $CD8^+CAR^+$ T cells were sorted. Cells were co-cultured with $CD19^+$ K562 targets at a 1:1 effector-to-target ratio. After 16 h of stimulation, $CD19^+$ K562 cells were depleted using CD235a magnetic microbeads. Negatively selected $CD8^+CAR^+$ T cells were stained with Cell-Membrane 405 and AF647 anti-CD8, resuspended in complete cytokine-free AIMV medium, and loaded onto a single-cell barcode microchip. IsoLight data were processed with IsoSpeak, and high-dimensional single-cell analyses were performed using the CRUSTY web tool.[23]

Polychromatic flow cytometry

Ten- and 23-color flow cytometry panels were used to assess CAR T cell status from the infusion product through 1 year post-transfer. Cryopreserved PBMCs were thawed in RPMI supplemented with 10% FBS, penicillin (100 U/mL), streptomycin (100 μg/mL), L-glutamine (2 mM), and HEPES (20 mM). Cells were washed in PBS, stained with Zombie Aqua for 15 min at room temperature (RT), and surface-stained in a 1:1 FACS buffer (PBS, 2% FBS). Chemokine receptors were stained for 20 min at 37°C, and remaining surface markers for 20 min at RT. Intracellular staining for Ki67, T-bet, GZMB, and GZMK was performed using the FoxP3 transcription factor staining buffer set, with antibody incubation for 30 min at 4°C. Data were analyzed using the CRUSTY web tool.[23] Slingshot was applied after dimensionality reduction and clustering to infer continuous, branching differentiation trajectories.[39] Wishbone was used to enhance resolution of cell-state transitions, and derivative analysis refined temporal ordering of differentiation events. PCA and balloon plots were generated using custom Python scripts with Matplotlib and Seaborn.[40]

CAR T cell longitudinal tracking via integration site analysis

The frequency and genomic loci of retroviral CAR integration sites were assessed for each T cell memory subset obtained from infusion product and post-infusion samples. Cryopreserved samples were thawed in complete RPMI. After washing with PBS, cells were stained with Zombie aqua Fixable Viability Dye. Chemokine receptors CD95 and CCR7 were stained for 20 min at 37°C, while CD3, CD8, CD45RA, and CD45R0 were stained for 20 min at RT. $CD3^+CD8^+$ T cell memory subsets were sorted by FACS as follows: T_{SCM} cells ($CCR7^+CD45RA^+CD45R0^-CD95^+$), T_{CM} cells ($CCR7^+CD45RA^-$), T_{EM} cells ($CCR7^-CD45RA^-$), and T_{TE} cells ($CCR7^-CD45RA^+$). From each sorted memory subset, gDNA was extracted and subjected to whole-genome amplification. Integration site analysis was performed using a previously described method combined with high-throughput sequencing.[80] Sequencing reads were demultiplexed based on the sample-specific indices and analysis of sequencing reads including mapping and annotation to the hg18 version was performed using the IS-Seq bioinformatic pipeline.[80]

Anti-CAR immune responses

Serum samples were collected from patients pre- and post-CAR T cell infusion and anti-mouse CD19 CAR antibodies were quantified using an anti-CD19 (FMC63) CAR immunogenicity ELISA kit per manufacturer's instructions. Absorbance was measured at 450 nm and 630 nm using a Spark 10M multimode microplate reader (Tecan). To reduce background noise, the OD630 value was subtracted from the OD450 reading. A standard curve was generated using SparkControl software, and anti-mCD19 CAR antibody concentrations were calculated accordingly.

QUANTIFICATION AND STATISTICAL ANALYSIS

Statistical analyses were conducted using PRISM software v10.2.3 (GraphPad Software, La Jolla, California, USA). Comparisons between standard and T_{SCM}-enriched CAR T cells were conducted using the Mann-Whitney test. For comparisons involving three or more independent groups, one-way ANOVA (Kruskal-Wallis test), or multiple *t*-test with Holm–Šídák correction were used, as appropriate. The Wilcoxon test was employed for paired analyses. The chi-square test was applied to compare the rate of CRs. EFS curves were compared using the log-rank (Mantel-Cox) test. Pearson correlation was used to generate correlation plots. Statistical significance was indicated as follows: $*p < 0.05$, $**p < 0.01$, $***p < 0.001$, $****p < 0.0001$.

ADDITIONAL RESOURCES

This work is based on a completed phase I clinical trial (clinicalTrials.gov: NCT01087294, URL: https://clinicaltrials.gov/study/NCT01087294).

Supplemental figures

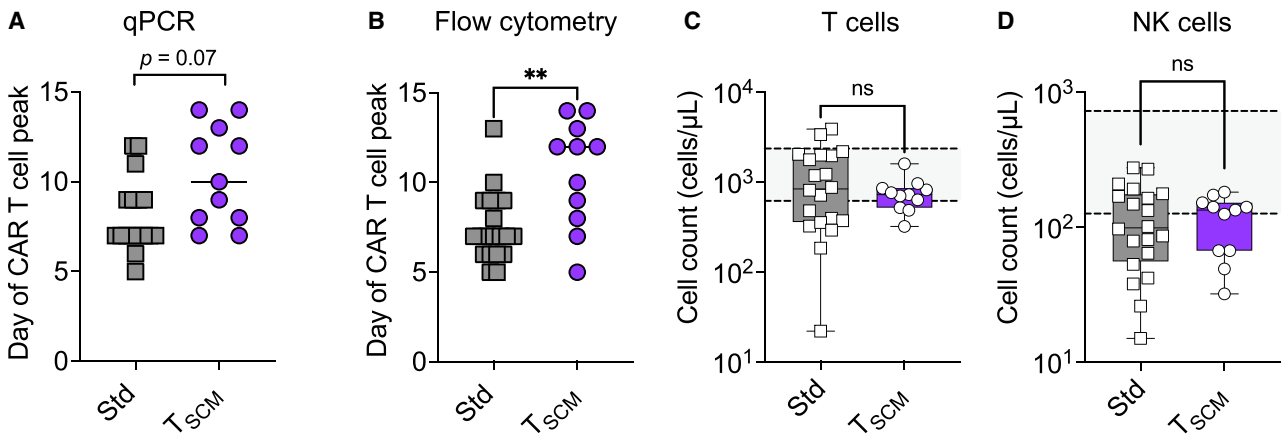

Figure S1. Distinct kinetics of CAR T_{SCM} cell expansion occur independently of baseline lymphocyte levels, related to Figure 2

(A and B) Day of peak of CAR T cell expansion measured by qPCR (A) and flow cytometry (B). Lines represent median values.

(C and D) Blood counts of T cells (C) and NK cells (D) immediately prior to CAR T cell infusion. $^{**}p < 0.01$ (two-tailed Mann-Whitney test); ns, not significant.

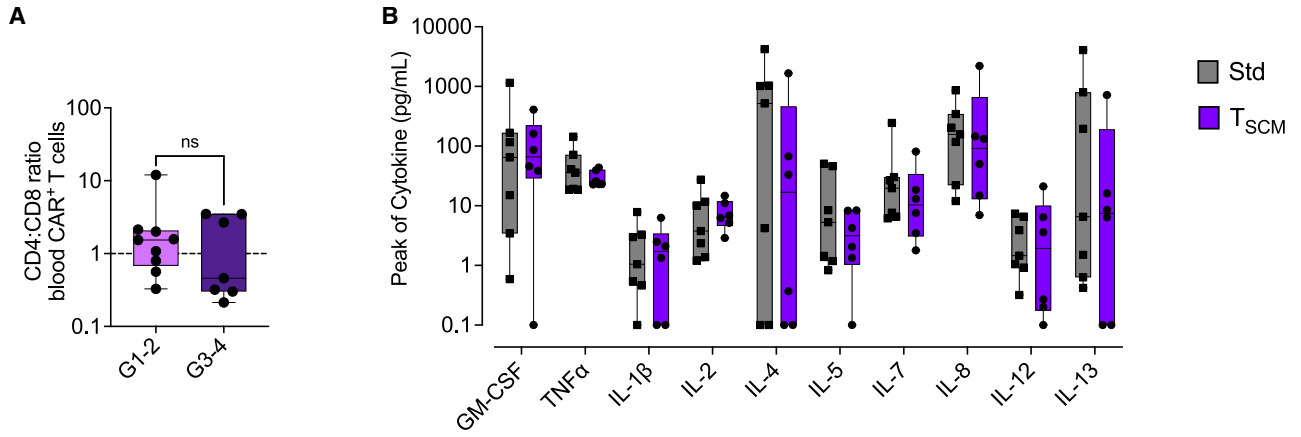

Figure S2. Immunological parameters not associated with CRS severity, related to Figure 3

(A) CD4:CD8 ratio at the peak of CAR T expansion in the blood of patients who received standard CAR T cells.

(B) Peak serum levels of key cytokines involved in CRS onset in responder patients within two weeks following infusion of standard or CAR T_{SCM} cells (standard $n = 7$; T_{SCM} $n = 6$). No significant differences were observed (multiple t test, Holm-Šídák correction for multiple comparisons).

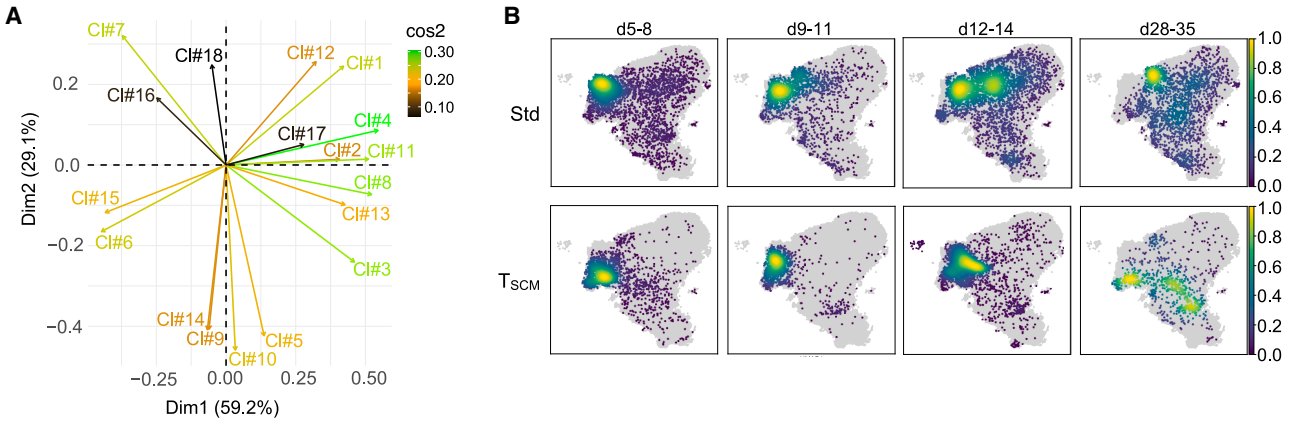

Figure S3. Trajectory mapping of CAR T cell differentiation *in vivo*, related to Figure 4

(A) Biplot showing cluster contribution to PCA based on cos2 values. Cos2 reflects the quality of variation in PCA, with higher values indicating greater contributions to the principal components. Vector lengths represent each cluster's contribution to the two principal components.

(B) Density plot representing the cluster dynamics of $CD8^+CAR^+$ T cells over time along the pseudotime trajectory shown in Figure 2B. The gray background represents total $CD8^+$ cells.

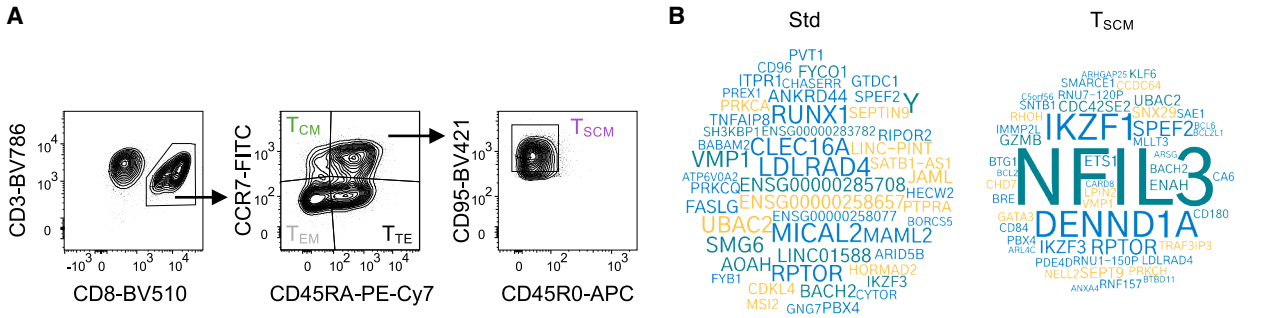

Figure S4. Diversity of CAR T cell infusion products, related to Figure 5

(A) Gating strategy for a representative patient (Pt #15) employed to isolate each T cell subset for integration site analysis.

(B) Word clouds displaying the top 50 represented ISs loci in the CAR T cell infusion products in Pt #15 (standard, left) and #22 (T_{SCM}, right). Each locus is labeled with the name of the closest gene to the relative insertion site. The size of each gene name is proportional to the number of integrations found at that locus, with larger fonts indicating higher integration frequencies.

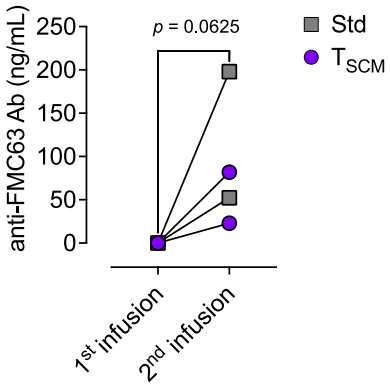

Figure S5. Enhanced humoral immunity against CARs following the second CAR T cell infusion, related to Figure 6

Patient serum levels of anti-FMC63 antibodies measured after the first and second CAR T cell infusions (standard, Pt #9 and #18; T_{SCM}-enriched, Pt #21 and #29). One-tailed Wilcoxon test.